ASSEMBLY OF

HYDROXY APATITE: β TRICALCIUM PHOSPHATE:

CALCIUM SULFATE BONE ENGINEERING SCAFFOLDS

By
CORNELIA E. CRETIU VASILIU
Bachelor of Science and Engineering of Oxidic Materials
"Babes-Bolyai" University
Cluj-Napoca, Romania
2001

Submitted to the Faculty of the
Graduate College of the
Oklahoma State University
in partial fulfillment of
the requirements for
the Degree of
MASTER OF SCIENCE
December, 2008

ASSEMBLY OF

HYDROXY APATITE: β TRICALCIUM PHOSPHATE:

CALCIUM SULFATE BONE ENGINEERING SCAFFOLDS

Thesis Approved:

Dr. James Earl Smay

Thesis Adviser

Dr. Khaled A. M. Gasem

Dr. Marty High

Dr. A. Gordon Emslie

Dean of the Graduate College

To Lucian

AKNOWLEDGEMENTS

My deepest gratitude goes to my parents Elisabeta and Corneliu-Ionel Vasiliu of Bistrita, Romania, for their upbringing which seeded in me the need for better and best. My husband Lucian is the one to whom I dedicate this work. Without his unmoving belief in me and his courage to embark with me in this long quest for more knowledge I could not have accomplished anything. I also want to give my gratitude to my friends Alin and Delia Dobra of Gainesville FL, for all their help that got me into graduate studies.

I owe special thanks to my adviser, Dr. James Earl Smay for his patience and direction. He offered me a fertile environment to grow intellectually and opens for me doors towards new achievements. To Elizabeth Clark from New York University, Department of Biomaterials and Biomimetics, I'm indebted for help, inspiration, patience, and friendship. Special appreciation goes towards Dr. Khaled A.M. Gasem whose input in my studies inspires me as a model of professor.

I'm giving my appreciation to the community from The Wesley Foundation at OSU. Their constant help and support made this endeavor possible. To my colleagues Eric Whitebay, Jing Shyan Chen, and Xu Jian I want to thank for being next door whenever I needed them.

Last, and not least I want to thank to my colleague, brother-from-another-mother and-father, Ben Lawrence and all the Lawrence and Curtis family for demonstrating that family is not always just the people that have the same blood running through their veins.

TABLE OF CONTENTS

TABLE OF FIGURES

INDEX OF TABLES

NOMENCLATURE

2-D:	Two dimensional
3-D:	Three dimensional
BCP:	Biphasic Calcium phosphates
CAD:	Computer aided design
CaS:	Calcium sulfate
Ch:	Chitosan
FDC:	Fused deposition of ceramics
FDM:	Fused deposition modeling
HA:	Hydroxyapatite
SEM:	Scanning electron microscopy
SFF:	Solid free form fabrication
USFDA:	United States Food and Drug Admnistration
XRD:	X-ray diffraction
βTCP:	Beta-tri Calcium phosphate

CHAPTER 1

1.0 INTRODUCTION

The overarching objective of this thesis project is to utilize the capabilities of solid freeform fabrication (SFF) of hydroxyapatite (HA) and β-tricalcium phosphate (βTCP) to engineer scaffolds that support the regeneration of bone in humans. Modern medicine has advanced tremendously in the last century. Bone repair techniques have developed from amputation and wood splints to artificial Titanium and High Density Poly-Ethylene joints. No matter how advanced these techniques may be, there are still situations when bone tissue itself needs to be helped to repair larger defects. Bone grafting is a good solution for these cases but is limited by the amount of bone tissue that can be harvested from a person (autografts) or by immunogenic reactions if tissue is harvested from another person or species (allografts and xenografts). Unlike other types of grafts, artificial grafts in the form of bone scaffolds are not limited in available quantity and do not raise any immunogenic response from the human body. Calcium phosphate-based bone scaffold products are already on the market in various forms: solid, particulate, and cements.

New ways of manufacturing these scaffolds, like solid free-form fabrication (SFF) techniques, and a deeper understanding of how the human body interacts with the artificial grafts, open new directions of research. The research motivation is two-fold: (1) To better understand the relationship between processing, structure and properties of bone scaffolds, and (2) to improve the quality of patient care by shortening recuperation time and the range of damage that can be treated.

1.1 Objectives

Solid freeform fabrication of bone scaffolds offers the ability to spatially control composition within a designed, three-dimensional (3-D) porous structure and to achieve varied temporal and spatial dissolution behavior. Filling the HA-βTCP scaffold pore volume with soluble biomaterials (such as calcium sulfate (CaS) and chitosan (Ch)) augments scaffold behavior in two ways. First, the filler prevents the creation of initial blood clot in the otherwise open pores of the scaffold reducing the likelihood of infection in these stagnant regions. Second, the filler phase can be used to release drugs such as growth factors and antibiotics at a controlled rate from the implant.

The present thesis is organized in five chapters. The first chapter states the objectives of this study and offers background information from the available literature on the topics of bone tissue, bone scaffolds, materials for bone scaffolds and their properties, and an overview on manufacturing techniques for bone scaffolds. The second chapter introduces the working hypothesis. Chapter 3 describes the materials and methods used to assemble open HA-βTCP empty and filled scaffolds. Chapter 4 presents the results of powder processing, SFF assembly, and scaffold characterization. Chapter 5 discusses the implications of the results on potential bone replacement products and offers perspective on future research directions.

1.2 Background

1.2.1 Bone tissue

Human bone is a dynamic, living organ. A complex, porous bio-composite, bone creates the environment for osteogenesis, osteolysis, hematopoesis, and also serves as a calcium reservoir for the body, [1]. Structurally, bones consist of HA nanocrystals in a collagen matrix with an intercalating pore network. The density of bone (*i.e.*, amount and structure of porosity) varies spatially depending on the primary function of the bone. Around the periphery, known as cortical bone, density is high (*i.e.*, high mineral content and low porosity) where structural support is key. The interior of bony structure, the cancellous bone, is often referred to as "spongy" in reference to the relatively open and compliant structure, [2]. The architectural units (similar to support beams) of the bone tissue are called trabeculi and they measure from 130µm to 350µm in diameter. The open porosity provides pathways for vascularization and nutrient flow.

In a healthy human, bones are resilient vital organs of the body that constantly remodel and repair. However, trauma to the skeletal system by accident, osteoporosis, surgical removal of tumors and other diseases often overwhelm the ability of bone to self-heal. These types of defects that cannot heal without intervention are called critical defects. In the United States, it is estimated that over six million bone fractures occur each year with 5-10% of these cases resulting in delayed healing or nonunion, [3]. When the body cannot heal itself, physicians have two options: amputation or augmentation of self-healing by implantation of bone grafts or artificial scaffolds.

1.2.2 Bone scaffolds

Annually, more than 500,000 bone grafting procedures are performed in the US. Grafts for bone defects are common in dentistry to stimulate bone regeneration around fresh socket dental implants, [3]. While highly successful, these grafts often depend on harvesting living bone from a second surgical site on the patient (autograft), from another person (allograft), or from another species (xenograft) (See Introduction, page 1). The use of porous HA as a scaffold onto which natural bone may grow has gained popularity in the medical community due to its biocompatibility, ease of use, and elimination of bone harvesting from a second surgical site, [4].

Both HA and βTCP are members of a larger family of calcium phosphates and have been approved as biomaterials by United States Food and Drug Administration (USFDA). βTCP is sometimes preferred because it is soluble. Scaffolds fabricated from HA can stimulate regeneration of bone across large gaps, [5]. They have been used for many applications, including skull, [6], facial bones, [7], and alveolar ridges of the jaw, [8]. Previously scaffolds were in granular or block forms which are difficult to shape. The particulate form can conform to the geometry of a surgical site. However, the particulates often migrate, resulting in voids and vulnerability to infection.

While calcium phosphate ceramics appeared relatively recently on the list of bone repair materials, calcium sulfate (CaS) has been used for 106 years being reported ever since 1892, [9]. CaS is an effective soluble bone repair material which is known to stimulate bone repair by causing local precipitation of a biological apatite “trellis” for bone conduction. It has also been shown to be stimulating the growth of blood vessels and to cause high levels of local bone formation and remodeling activity. It erodes from

outside inward by surface dissolution, and it has been shown to dissolve at a rate of ~1mm per week. Lately it has been used successfully as a carrier to release growth factors or antibiotic, [10, 11]. The major shortcomings of CaS are that it degrades *in vivo* at a relatively fast rate (faster than bone can grow into larger defects) and it lacks mechanical strength.

Another biomaterial used for drug release is chitosan (C). This material is obtained by deacetylation of the natural polymer chitin found in crustaceans. It is also known to be biocompatible and bioactive, [12], and has a degrading mechanism based on lysozyme *in vivo*. The final degree of deacetylation dictates some of the properties of the material, [12].

The composition of the scaffold material is important at the cellular level. Previous studies, [13-16], show that the following concepts are important for the kinetics of mineralized tissue formation: pore size variation, pore connectivity, surface properties, and composition. There are four dimensional scales where interaction between body and material happens: (1) nano-scale, (<1µm), where the chemical structure of the material plays the most important role, chemical reactions, mineral and protein interactions take place here, (2) micro-scale, (1-20µm), which primarily influences the way in which cells interact with surfaces, (3) meso-scale, (20µm to 1000µm), that primarily influences the way in which tissues interact with surfaces, and (4) macro-scale, (>1mm), that primarily influences the way in which anatomy (organs) interact with implantable devices. Until recently, the control of micro and meso-structure has been dependant on the manufacturing process, which made it impossible to assess the role and limits of cellular and tissue response to architecture-related variables.

Consequently, the optimization of HA scaffolds remains important in biomaterials research. Key questions about the amount, size, and structure of porosity (nano/micro/meso/nano) in scaffolds remain unanswered, [17, 18]. Orthopedists would prefer to use scaffolds that allow natural bone structure to reform as the scaffold is metabolized by bone cells and eroded by body fluids. HA is virtually insoluble. Hence, bioglasses and soluble βTCP have gained in popularity, [19-21]. The βTCP phase undergoes dissolution and reprecipitation in the body, produces a carbonated apatite; the resulting material is replaced during bone formation and remodeling.

To summarize, bone scaffolds are artificially manufactured structures that help in the healing process of bone tissue. The healing is dependent on the composition and architecture of the scaffold. From the compounds that can be used for the fabrication of these structures, calcium phosphates in the form of HA and βTCP proved to perform well in clinical studies. They were approved by USFDA as biomaterials. Other materials that can be used, like CaS and Ch, can double as drug delivery vehicles. More in-depth information on these materials and the manufacturing techniques for fabricating scaffolds follow in the next sections.

1.2.3 Calcium phosphates

Calcium to phosphorus ratio in naturally occurring bone varies from 1.67 to 1. Of particular interest for artificial bone scaffolds are those phosphates with calcium to phosphorus molar ratios of 1.5:1 (TCP, $Ca_3(PO_4)_2$ and 1.67:1 (HA, $Ca_{10}(PO_4)_6(OH)_2$) as shown in Figure 1, [22]. Note that this phase diagram only represents the de-hydroxylated calcium phosphates and the mole percentage of CaO relative to P_2O_5 is the metric for

distinction. In the figure C stands for CaO and P stands for P_2O_5. The binary mixture corresponding to $C_{3.3}P$ composition is equivalent to HA and is situated in the dark shaded segment of the diagram. The C_3P composition is equivalent to the TCP compound (which was initially accidentally produced in cases where making HA and components were deficient) and is situated at the boundary of the dark shaded and lighter shaded areas.

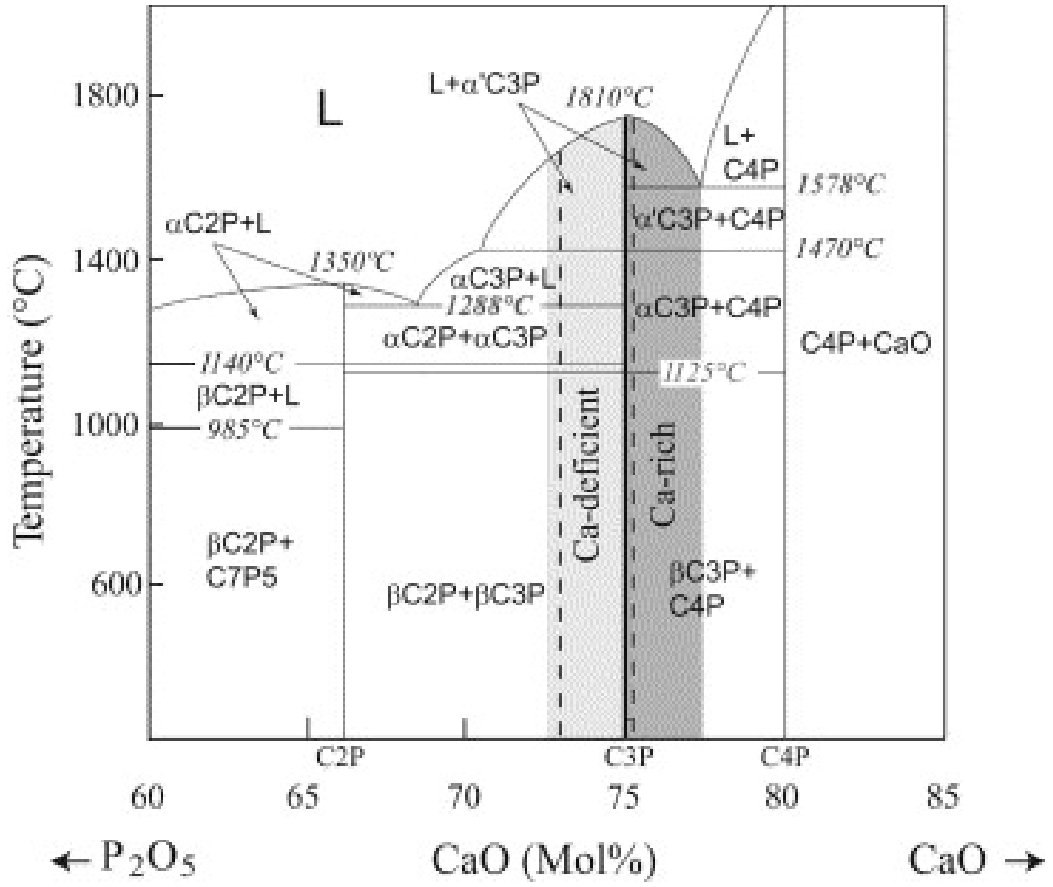

Figure 1 Phase diagram of calcium oxide- phosphate binary system [23], molar percentage of CaO in bynary $CaO+P_2O_5$ combinations versus temperature in degrees Celsius. C corresponds to CaO and P corresponds to P_2O_5, all nomenclature is done accordingly: C3P corresponds to tri-calcium phosphate, [24].

As shown in Figure 1, a rise in temperature causes solid state phase transformations. For Ca deficient C3P, a liquid phase is present above 1288^{o}C whereas

for Ca rich C3P, liquid is present above 1578^{o}C. The relative difference in the eutectic temperatures for these systems indicates that Ca deficient C3P (i.e., βTCP) should sinter at a relatively lower temperature than Ca rich C3P (i.e., HA). The missing caveat of this argument is the effect of the hydroxyl component on sintering or phase behavior. However, it is assumed that at the elevated temperatures of sintering, it is the behavior of the de-hydroxylated oxides that will be important.

In contrast to the synthetic apatites, biological apatites (naturally occurring in live organisms) are rarely stoichiometric, incorporating "impurities" in the form of other metals ions for Ca^{2+}, [22, 25]. The most common form of HA appears in hexagonal crystalline form with lattice parameters a=b=9.422Å and c=6.883Å (Space group $P6_{3/}m$-hexagonal closed packed), [26, 27]. HA has a solubility product at pH~7.3 (body conditions) of $2.35x10^{-59}$($K_{sp,}$(mol/kg)^{n}, where n=18), [22].

ß-Tricalcium phosphate (β-TCP, β-Whitlockite), $Ca_3(PO_4)_2$, is also biocompatible. It is found in many cases to be advantageous compared to HA as a biomaterial, due to its higher resorbability. Its solubility product is $2.83x10^{-30}$ (K_{sp},(mol/kg)^{n}, where n=5) a few orders (29) of magnitude larger then HA's solubility product (see Figure 1), [22].

Biphasic calcium phosphate or BCP consists of a mixture of HA and βTCP in varying ratios as a nano/micro composite [28]. Co-sintering of particulates of both is carried out at temperatures where the diffusion of Ca from rich to poor regions is slow and the two phases remain distinct. BCP preparation was described in 1986 by R. LeGeros, [29], and the *in vivo* properties characterized in collaboration with a group conducted by G. Daculsi, [30, 31]. According to these studies, BCPs as biomaterials

have controlled dissolution, and due to the material's chemical composition, the bone ingrowth is done at the expense of ceramic. BCPs are obtained when a quantity of biological calcium deficient apatite is sintered at temperatures above 700^{o}C. The BCPs' reactivity is determined by the HA/βTCP ratio: the lower the ratio the higher the reactivity, [32]. The BCP materials *in vivo* and *in vitro* produce responses from bone cells that are the same as bone material: cell attachment and proliferation, [33]. The BCPs commercially available are shaped in blocks, particulates or in the form of injectable material in a polymer carrier.

Whatever the composition of the implant (HA, or βTCP, or a mixture of both), the bone tissue reaction follows the same cascade of events observed in fracture healing. This cascade includes: (1) hematoma formation, (2) inflammation, (3) neo-vascularization, (4) osteoclastic resorption, and (5) new bone formation. Macrophages are the major infiltrating cells when HA and βTCP are implanted. These cells secrete hydrogen ions and degrade the ceramics. Specific proteins are secreted in human fibroblasts with HA particles. Osteoclasts fragment the material even further and the particles are remodeled by the osteoblasts which are the cells that secrete new bone material. Adding cells or bioactive materials such as bone morphogeneic protein (bone growth factor) can enhance bone integration. The remodeling part of the process occurs naturally in the bone: the whole skeleton remodels completely in a period of three years, [34].

From the family of calcium phosphates, HA and βTCP are biocompatible and bioactive. They are known to induce bone growth and bone tissue differentiation when implanted in a living body. Due to their studied properties, both of the materials were approved as biomaterials by the USFDA. Different products that contain one or both

materials can be found on the market in different forms of presentation: particulates, cements, or solid blocks. Whatever the shape, when implants are introduced in the body, a process of integration takes place. The integration follows the same steps as a fracture healing. In this process, the blood first occupies the empty pores and blood clots form. The inflammation that follows the blood clot formation can hinder the healing process. To reduce the inflammation and prevent space for infection, soluble fillers could be used to close the porosity temporarily, dissolving to allow a gradual in-growth of the tissue. These fillers could also carry drugs -antibiotics or growth factors- that could help in the integration process. The following section of the thesis is dedicated to some of these fillers.

1.2.4 Biodegradable and soluble fillers

Scaffolds require interconnected pore networks to not only stimulate osteoblast migration and osteoconduction, but also to permit sufficient nutrient support to the cells within the scaffold. With an open weave porous scaffold, trapped blood coagulates to produce a blood clot that can induce inflammation, potentially house an infection, and possibly result in rejection of the scaffold, [3].

The idea of filling the scaffold with a temporary material is to reduce, if not to prevent, the blood clot formation, and to leave no site for infection. The material must last for a limited time to allow both for the construction of a viable network of blood vessels in the porous structure that is revealed by the dissolution of the filler, and for bone cell infiltration and matrix formation. For this, a relatively fast dissolving, biocompatible, biodegradable material is required. There are several possible candidates

from which CaS and C were selected due to their good integration of bone from numerous previous studies, [10-12, 35-38].

Calcium Sulfate Hemihydrate ($CaSO_4 \cdot 0.5H_2O$ (CaS)) is one of the oldest materials that were implanted in a human body. Calcium content and its high solubility make it viable candidate for soluble filler, [39, 40]. CaS mixed with water at normal (ambient) temperatures converts chemically to the more stable dihydrate form, while physically "setting" to form a rigid, relatively strong gypsum crystal lattice, [41]:

$$CaSO_4 \cdot ½H_2O + 1½\ H_2O \rightarrow CaSO_4 \cdot 2H_2O \quad (1)$$

The dihydrate has a solubility product of $4.93x10^{-5}$(K_{sp} $(mol/kg)^n$, where n=2), much more soluble compared to HA and βTCP (25 orders of magnitude bigger than βTCP's K_{sp}, 54 orders of magnitude bigger than HA's). CaS resorption in a living organism has been registered to be approximately 1mm per week, [3].

An organic material that is a good candidate for filler is chitosan (Ch). Ch is a polysaccharide derived from N-deacetylation of chitin using (usually) sodium hydroxide. Chitin is a biopolymer present in nature primarily in the outer shell of crustaceans and mollusks, in the backbone of squids and the cuticle of insects, [42, 43]. Composed of β (1-4) linked 2-acetamido-2-deoxy-D-glucose and 2-amino-2-deoxy-D-glucose, the Ch is a semi-crystalline polymer, the degree of crystallinity being dependent of the degree of deacetylation, [44]. A higher degree of deacetylation will yield a more soluble product. Ch is soluble in aqueous acids (pH<6.3), and it is possibile to shape this material in fibers or other shapes (films, etc.) by depositing the hydrogel in a high pH solution. The gel obtained by dissolving the Ch in a weak acid solution can also be used to fill the micro and meso-porosity of a scaffold. In the polymer structure, molecules of antibiotics or

other drugs can be encapsulated to be released when cells metabolize the polymer filling. The enzymatic degradation mechanism with lysozyme makes this polymer one of the major materials for tissue engineering due to its biocompatibility and biodegradability. Also, the minimal immune reaction and cell growth promotion make it a top competitor for soft tissue repair and bone regeneration, [45].

The purpose of the fillers is to increase the mechanical strength of the scaffold, and to prevent blood clot formation and the subsequent inflammation of the surrounding tissue. Another possible purpose of using fillers is drug delivery at the implant site. Although they can be used as implant materials in their own right, filler materials are introduced to improve the scaffold. The scaffold fabrication techniques are the subject of the following section of literature review.

1.2.5 Fabrication methods

There are numerous fabrication techniques to assemble porous bio-scaffolds, but the most common examples are: electrospin casting, [46], foam-gel technique, [47], particulate leaching, [48], emulsion freeze drying, thermal phase separation, [49], fiber bonding, membrane lamination, melt molding, fused deposition modeling, and solid freeform fabrication, [45, 50]. Each technique has limitations such as the poor meso-pore size control, limited structure composition design capabilities, and uncertain pore interconnectivity, among others. Some of these techniques are succinctly described in the following paragraphs.

The foam-gel technique involves a cross-linking polymerization that gels the foam-like HA slurry rapidly. HA is mixed with a crosslinking substrate (poly-ethyleneimine) and then with a foaming agent. A poly functional epoxy compound is

used to gelatinize the foamed slurry. The gel can be poured in molds, dried, and sintered. The final product has an interconnected porous structure which gives favorable results in clinical studies (all implants were completely incorporated 6 months after implantation), [47].

Another technique is fused deposition modeling (FDM) which assembles three dimensional (3-D) models by extrusion, patterning, and solidification of a molten polymeric filament. If the thermoplastic filament is loaded with ceramic particles, the process is dubbed fused deposition of ceramics (FDC), [51-53]. Deposition speeds are relatively slow and 3-D pore architecture is somewhat difficult to control. Additionally, the large polymer content requires extended binder burnout steps when producing an oxide ceramic structure. Another disadvantage of fused deposition modeling is that this process requires high operating temperatures. As a result, patterning of many biological materials is precluded. Current FDM implementations have shown little ability to grade composition throughout the 3D build volume. Nevertheless, this technique has processed poly(e-caprolactone), polypropylene-TCP, poly(e-caprolactone)-HA, and other biomaterials. FDM/FDC is a viable technique for assembling bone scaffolds directly [54]. Variations of the FDM technique are: the three-dimensional fiber-deposition technique, precision extruding deposition, and precise extrusion manufacturing.

Current forming technology for bone scaffolds produces a homogeneous pore structure, often by a templating method. This provides a generic shape for the surgeon to artistically trim and place in the wound site, [4, 55-57]. Solid freeform fabrication (SFF) has only recently been used to reproduce bone-like structures and has been proposed as a means to create custom geometries to repair specific wounds without requiring bed-side

shaping, [55, 58]. Computer aided SFF offer the possibility of customized geometry, porosity and composition scaffolds for an individual patient. SFF methods, such as: FDM, selective laser sintering, laminated object manufacturing, lost mold techniques, stereolithography, and 3-D printing or robocasting, exhibit a precise control over architecture.

The lost mold technique is an indirect scaffold fabrication route. A thermoplastic polymer mold is created by machining or SFF. Subsequently, a mixture of organic binder and ceramic is injected to fill the mold cavities. The filled mold is then immersed in an appropriate solvent to remove the mold. The green body obtained is sintered. The accuracy of the final product depends entirely on the precision of the mold, [59]. The nature of the process is the production of homogeneous composition throughout the structure and limitations on 3-D architecture. The indirect methods conserve the physical, chemical, and mechanical properties of the biomaterial because these materials do not undergo the rapid prototyping process; they are added to the scaffolds later in the process.

Stereolithography, like FDM, fabricates structures using a mix of ceramic powders in a polymeric matrix. The ceramic suspension is photocured, layer by layer, fabricating a three-dimensional ceramic green body. Subsequent binder removal results in a sintered ceramic part, [60]. This process is also capable of making polymer molds for the indirect scaffold formation method.

Robocasting, [23, 24, 61], is the SFF low temperature technique that uses concentrated colloidal gels as inks for the direct write process though extrusion. Layers of intricate 2-D patterns are deposited one upon another, leading to the desired architecture. Macro-pore size can be accurately controlled as well as the internal structure of the

scaffolds. The printing ink is obtained by dispersing ceramic powder in water with the aid of one or more polymeric dispersants to obtain a high concentration, low viscosity slurry. Next, a counter electrolyte is added to flocculate the particles into a colloidal gel with pseudo-plastic rheollogy.

Ink formulations made out of HA and βTCP are documented in literature, [23, 54, 62]. The formulations follow the same steps: first the ceramic particles are dispersed in water with the help of a dispersant (adjusting the pH or not), then a thickening agent is added (with or without an antifoaming agent), and finally the suspension is gelled. Colloidal gel inks for the robocasting process need to satisfy two important criteria. First, they must be able to flow through fine deposition nozzles (Ø200μm) maintaining their shape and elastic properties when extruded into 3-D patterns. Second, they must possess a high solids concentration to resist drying stresses and prevent cracking and warping, [63]. Defects (such as cracks) alter the mechanical strength of the structure reducing significantly the load-bearing capacity or even the integrity of the scaffold during the implantation process. Warping alters the overall shape of the implant making it difficult to fit perfectly the prescribed dimensions.

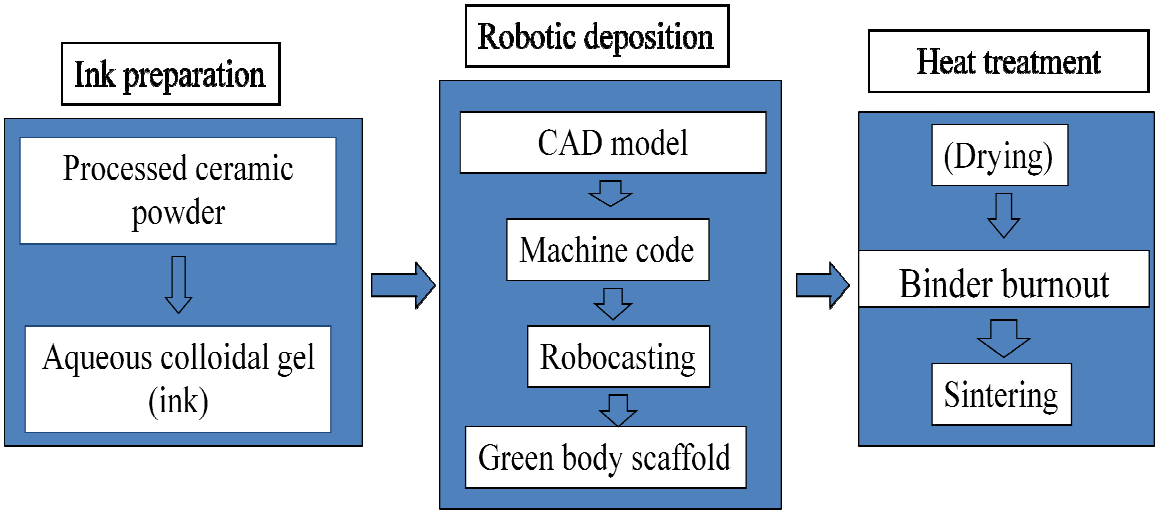

Figure 2 Diagram of ceramic scaffold fabrication flowchart

The flowchart of the fabrication process is represented in Figure 2. First, the ink preparation includes a processing step for the as-received ceramic powder. Stable, small particles of ceramic are obtained through calcination and attrition milling. The colloidal gel formulation follows. The ink thus obtained is then extruded through a fine nozzle in the pattern and dimensions desired by robotic deposition. Tool path calculation begins with a computer-aided design (CAD) code. The machine executes the code (x,y,z linear interpolation) depositing the extruded filament in the desired pattern. The green body ceramic obtained at the end of the robocasting process needs to be heat treated to reach its final dimensions, strength, and density. First, the structure dries at room temperature (or in a low temperature oven) and then is heated to burn out the polymer binder and sinter the ceramic particles.

A schematic of the robocaster (gantry robot with extruder(s)) can be seen in Figure 3(a). The gantry traces the extrusion nozzle affixed to the z-axis through tool paths in the x-y plane. Deposition may be through a nozzle(s) directly attached to the syringe(s) or by

directing the inks through a mixing chamber and then through the deposition nozzle (see Figure 3). Spatial variation of composition, [58, 63], is possible by feeding two or three inks into a mixing chamber. As deposition proceeds, each syringe pumping rate can be controlled to blend any desired composition. The separate nozzle variation offers the possibility of constructing elements of the structure from different materials (an example could be a layer by layer design in which alternate layers of three different materials -A, B, C- can alternate in any desired order). Deposition is done in a paraffinic oil bath to prevent drying of the structure during fabrication.

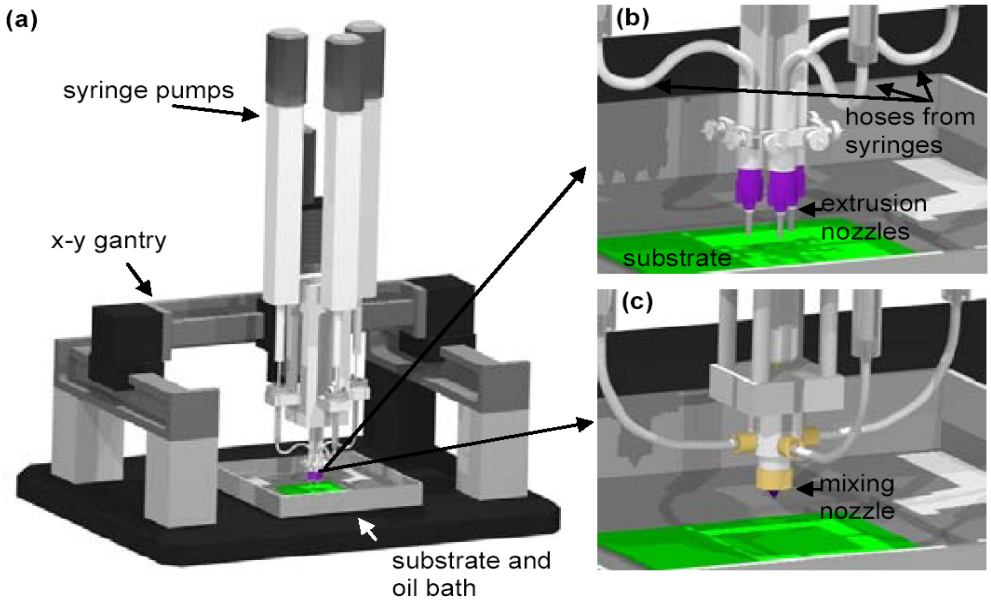

Figure 3 Computer-generated image of the robocaster with details: (a) schematic overview of the gantry robot, (b) deposition through separate nozzles, and (c) deposition through mixing chamber-nozzle assembly

Robocasting is limited by the complexity of programming involved in fabricating varied geometries. In order to create complex geometries a new improved code is needed. Improvements in programming language and a friendlier interface might solve some of

the problem. Another problem is choosing the right size of nozzle for printing. The dimension of the printing nozzle is linearly related to the dimension of the particles suspended in the polymer carrier. The dimension chosen for printing has to be larger than the desired dimension of the struts, taking heat treatment shrinkage in consideration. The ceramic struts after sintering need to be comparable in diameter with the bone trabeculi.

CHAPTER 2

2.0 HYPOTHESIS

2.1 Hypotheses Statements

(1) Three-dimensional, binary hydroxyapatite and beta tri-calcium phosphate scaffolds may be printed using high particle concentration, printable aqueous inks and the green body may be sintered successfully to retain both mineral phases in the final product.

(2) HA-βTCP scaffolds with a higher percentage of βTCP, the more soluble phase, dissolve faster in simulated body fluid than scaffolds with a high HA content.

(3) Sintering conditions influence shrinkage, density, porosity and dissolution rate for the scaffolds regardless of HA to βTCP ratio.

(4) Increasing the overall porosity in the scaffolds by introducing a porogen in the printing step increases the rate of dissolution in simulated body fluid.

(5) Scaffolds with CaS filled pore space will dissolve in two stages where the filler will rapidly dissolve first, followed by the gradual dissolution of βTCP in simulated body fluid.

2.2 Hypotheses Tests

To test the hypothesis (1), the mineral composition of the ceramic powder is confirmed by x-ray diffraction before and after calcinations and also after densification of the printed structures. Second, particles size distribution of the ceramics for the ink formulation is assessed by dynamic light scattering. Third, printability of the resulted inks

is tried by robocasting. Fourth, the degree of sintering and morphology of the heat treated samples is assessed by scanning electron microscopy. Finally, three mixtures of HA and βTCP are formulated as inks and the dissolution characteristics of the resultant structures are analyzed *in vitro*.

To test hypothesis (2), dissolution behavior of prepared scaffolds is measured by weight loss measurement as a function of time in simulated body fluid. Hypothesis (3) dissolution behavior is tested in a similar way and the sintering conditions effect on shrinkage is observed by treating ceramic samples made out of the same composition at various temperatures in the interval 1100 to 1200^{o}C for a constant duration of time. Linear dimensions are measured before and after sintering, resulting the shrinkage. Porosity and density are measured via Archimedes's method and dissolution behavior is obtained by gravimetric method *in vitro*. The third hypothesis is proved by analyzing the dissolution behavior of sintered samples fabricated from mixtures of ceramic and fugitive inks in various proportions. The effect of the amount of fugitive materials on surface morphology will be analyzed by scanning electron microscopy. The last part of the hypothesis refers to the CaS filler. CaS evolution during dissolution is followed by measuring the weight of the samples in time. Scanning electron microscopy is performed on samples retrieved during the dissolution study and at the end of it.

CHAPTER 3

3.0 MATERIALS AND METHODS

Assembly of HA:βTCP composite scaffolds by SFF is a multi-step process involving ink preparation, printing, sintering, and filling with CaS or chitosan. For ink preparation, the as-received ceramic powders are first calcined and milled to obtain smaller, more uniform particles. Next, the ceramics are dispersed into water and controllably flocculated to form the colloidal ink used for robocasting. The as-printed green-body ceramic scaffolds are then heat treated to burn out the polymer binder and sinter the particles. Finally, the fillers are prepared in a slurry or gel form and infiltrated into the pore space of the scaffolds. The result is a filled ceramic scaffold that can be characterized *in vitro* by studying the dissolution behavior in simulated body fluid. This chapter describes, in detail, all the processing steps and methods used to fabricate and characterize the produced scaffolds.

3.1 Ceramic ink preparation

In order to obtain desirable printing characteristics of the colloidal inks, several pre-processing steps are required. The ceramic powders pass through calcination, attrition milling, and drying prior to ink formulation.

3.1.1 Calcination and Attrition Milling

Commercially available powders of hydroxyapatite (HA) (Product 10185602, Lot 43640, Honeywell, Germany) $Ca_{10}(PO_4)_6(OH)_2$ and β Tri-Calcium phosphate (βTCP) (Product 21218, Lot 1305078, Sigma-Aldrich, Germany) $Ca_3(PO_4)_2$ are used as ceramic materials in this study. The as-received powders are calcined in an alumina crucible at

800^{o}C (for βTCP) or 1100^{o}C (for HA) for 11 hours. The powder is then attrition milled (0.9-1.1mm zirconia milling media, Union Process, Akron, Ohio) in ethanol (EtOH, analytic purity, Fischer Scientific, Product 241000200) for 3 hours (Model L001, Szegvary Attritor System, Union Process, Akron, Ohio). The suspension is then separated from milling media. The ethanol-ceramic slurry is centrifuged in an angled rotor at 8000rpm for 4 minutes in polycarbonate centrifuge tubes (Eppendorf 5660 Centrifuge). The ethanol separated this way is decanted and then the solid deposit is dried in an Oakton low temperature oven at 80^{o}C for 4-6 hours. The resulting solid material is then dry milled for 5 minutes on a paint shaker with zirconia milling media (10-20pieces of 10mm diameter milling media in a 500ml Nalgene bottle per batch). The powder is stored in a desiccator in a dedicated container.

3.1.2 Ink formulation

The calcined and milled ceramic powder is used for the ink formulation. Concentrated HA and βTCP suspensions, where volume fraction of ceramic $\phi_{ceramic}$=0.45 to 0.5, are produced by mixing an appropriate amount of ceramic powder and ammonium poly-acrylate (Darvan 821A, RT Vanderbilt, Norwalk, CT) solution to disperse particles into water. The optimal dispersant proportion per gram of ceramics is 14.5mg as determined by trial and error. The qualitative metric is that the suspension should become very fluid after a short (60s) mixing period upon addition of the powder to the dispersant solution. First, 10-15grams of milling media are added to the water, then the dispersant and then the ceramic powder in two parts (50%+50%). After each addition of powder the suspension is mixed in the conditioning mixer (Thinky AR-250, Thinky, Japan) for one minute. Next, hydroxypropylmethylcellulose (Methocel F4M, Dow Chemical Company,

Midland, MI) was added as a thickening agent. F4M is used in 5% by weight aqueous solution in a proportion of 7 mg of per milliliter of ceramic.

Table 1 Example $\phi_{ceramic}$=0.45 HA:βTCP=1:1 Ink Formulation

Substance	**Quantity** (grams)
DI Water	13.947
Darvan 821A	0.663
βTCP	20.925
HA	20.52
F4M (5%)	1.89
PEI (10%)	0.150

The suspension is then mixed for 1 minute and de-foamed for 30 seconds in the conditioning mixer. Finally, the suspension is gelled by adding 150-200mg per 30 ml of ink of poly-ethyleneimine (PEI, Product 195444, lot 9718C, ICN Biomedicals Inc., Aurora, OH) 10% by weight solution. Mixing and de-foaming (1 minute and 30 seconds, respectively) after the final addition finishes the ink preparation. The resulted ink needs to be printable through the desired size of the nozzle, which means the paste needs to be stiff enough to maintain the shape of the extruded filament after deposition but also soft enough to be extruded easily through the nozzle by applying a minimum amount of pressure.

3.2 Powder characterization

X-ray diffraction is performed on specimens of powder collected before and after calcination and after sintering, so that mineralogical composition can be confirmed. An X-ray diffraction system (Philips APD3520) is used to obtain spectra with Cu Kα radiation are analyzed in comparison with known, specific 2θ values for HA and βTCP.

3.3 Particle size analysis

Particle size analysis is done by three techniques: scanning electron microscopy (SEM), acoustic spectroscopy, and dynamic light scattering (DLS). Ceramic powder obtained by processing is mixed with ethanol to form 5% by weight solids suspension. For this, a calculated quantity of powder is weighted (PR5003 Mettler Toledo balance) into a plastic container. The appropriate amount of ethanol is added and then the suspension is mixed in the conditioning mixer (Thinky AR-250, Thinky, Japan) for two minutes. A drop of the resulting homogenized slurry is deposited on carbon tape, where it is left to dry in air at room temperature. Particle size and shape are then assessed through SEM visualization (JEOL JSM-6360).

In order to assess the particle size distribution in the processed ceramic powder, an acoustic spectrometer Model DT-1200 (Dispersion Technology Inc.) is used. For this, 175ml of $\phi_{ceramic}$=0.05 aqueous suspension is prepared. In a 250ml bottle (Nalgene) the right amounts of ceramic powder and deionized water were weighed. The slurry is then agitated for 10 minutes on a Red Devil paint shaker (Model 5400 Red Devil Equipment Co.). The slurry is then rapidly poured in the working chamber of the spectrometer, activating the peristaltic pump for continuous circulation. After setting the known data, such as density of the powder (ρ=3.04g/cm^3 for HA and ρ=3.11g/cm^3 for βTCP) and concentration of the slurry in the computer program that serves as an interface, the measuring cycle is activated. The resulted data can be expressed as frequency per particle size.

To assess the efficiency of the milling, particle size analysis is performed using dynamic light scattering (DLS). Samples of 2ml of slurry are retrieved during milling at 15 minutes intervals for 5 hours from the center of the mill, close to the mixing shaft using a single-use syringe. Light scattering was performed on the ceramic slurry samples using a high performance particle sizer (model HPP5001, Malvern Instruments). The DTS 3.0 program is activated, work temperature is set for 25^{o}C. Then, 1 ml of methanol is pipetted into the disposable low volume polystyrene cuvette (DTS0112), in which a small drop of the ceramic slurry (0.1ml) sample is added. The analysis sample rises approximately 11mm from the bottom of the cuvette. The cuvette is introduced in the designated place; lid closed and from the program interface “measure” command is called with the preset standard operation procedure set on the liquid medium (methanol). At the end of the measurement, the machine reports size distribution by volume with a particle average size, in nanometers.

3.4 Fugitive inks

3.4.1 Formulation

Rice starch ink is obtained by mixing a quantity of rice starch (Product S7260, Sigma Aldrich Inc., St.Louis, MO), to which a water dispersing acrylate is added (product number 28-618A, Elotex TITAN8100, Elotex Co.). Water is added to the mixture of powders, homogenizing for 2 minutes in the conditioning mixer (Thinky AR250, THINKY, Japan). Then a quantity of Pluronic F127 (Pluronic F127, BASF Co.) 25% water solution by weight is added. Slurry is mixed for 1 minute and de-foamed for 45 seconds two to three times. In the end, 500mg of Formaldehyde 10% by weight

aqueous solution is added for flocculation. The ink is mixed for another cycle of 45 seconds and de-foamed for 30 seconds in the conditioning mixer. The container is put to cool in iced water for 5 minutes before using it for printing.

3.4.2 Ceramic-fugitive ink mixtures

Volumetric mixtures of ceramic and rice starch ink are obtained. Separate single-use syringes (10ml, BD syringe) are filled respectively with ceramic ink and rice starch ink. The inks in the syringes are first de-bubbled of the incorporated air pockets. In a separate plastic cup, appropriate volumetric amounts of the two pastes are dispensed to formulate mixtures in the following proportions: 15% rice starch ink with 85% ceramic ink (for 10 ml of mixture 1.5ml of rice starch ink was mixed with 8.5ml of ceramic ink), 25% rice starch ink with 75% ceramic ink (10ml of this mixture contains 2.5ml of rice starch ink and 7.5ml of ceramic ink), and 50% rice starch ink 50% ceramic ink (10ml of mixture contains 5ml of rice starch ink and 5ml of ceramic ink).

3.5 Assembly of HA and βTCP scaffolds

Robocasting employs a gantry robot to extrude colloidal inks through fine nozzles in order to build three dimensional objects. Printing can be done with one or several materials either by using separate nozzles for each material or by using a mixing chamber prior to the deposition. The printing operation utilizes a motion and flow rate controlled deposition system. Colloidal inks are housed in syringes affixed to the *z* motion axis and connected to the deposition nozzle (see page 17 for schematics of the machine). A model of 3-D structure to be assembled is virtually sliced into layers and deposition tool paths are calculated using a CAD program. The layers are deposited (printed) sequentially,

starting with the bottom layer. After the printing operation, the structure is dried and sintered to yield a dense ceramic.

Periodic 3-D scaffolds are built via robotic deposition when ink contained in a syringe attached to the z-axis of the gantry robot (Aerotech Inc., Pittsburg, PA) is dispensed in the x-y plane. The robot utilizes CAD software (Robocad 3.1, 3-D Inks, Stillwater, OK). Samples are printed layer-by-layer at 6 to10mm/s deposition velocity in low viscosity paraffin oil to prevent drying of the structure during assembly. Once a layer is finished, the nozzle is translated up a programmable distance of 0.78D (D=inner diameter of the nozzle) and another layer is begun. This is repeated until the desired height of the structure is reached. Cylindrical nozzles (EFD Inc., Nordson, Westlake, Ohio) of 150-510µm interior diameter are used for extrusion. Since the post-sintering diameter for bone scaffolds is desired to be around Ø=250µm, Ø=330µm tips are considered ideal. The difference between the initial and final dimension of the struts is known as shrinkage and occurs when the water and/or binder are lost and sintering occurs.

3.6 Heat treatment

Heat treatment is essential for ceramics in order for these materials to achieve a reasonable mechanical strength. Here, reasonable means that the structures are capable of being handled in filling and implant operations. During this process, the fragile green body ceramic is densified and all organic components are burned away. Binder burnout and sintering causes volumetric shrinkage and, potentially, defects such as cracking and warping. The sintering shrinkage of ceramics is an unavoidable step of powder

processing and all dimensions of the green body structure must be enlarged to achieve the final desired dimensions.

The goal of the heat treatment processes is twofold. First, the sintering must strengthen the green body enough for handling during subsequent processes (e.g., filling pore space, *in-vitro* dissolution study, and implantation). Second, the amount and characteristic dimension of residual porosity within the scaffold rods (or struts) is dependent on the amount of sintering that occurs. Low temperature and short duration sintering promotes only neck formation between particles and, hence, a rather open, porous microstructure. As time and/or temperature are increased, the amount and size of residual porosity in the rods decreases. A typical firing schedule starts by heating at 2^{o}C/minute until 400^{o}C, a hold at 400^{o}C for 1 hour, then rapid heating till 900^{o}C (8.3^{o}C/min.), hold for 2 hours at 900^{o}C, heating 3.3^{o}C/min. to 1100^{o}C, then a hold at 1100^{o}C for 4 hours, and finally a rapid cooling at 9.1^{o}C/minute until the samples achieve room temperature. The influence of maximum temperature during the 4 hour soak is tested by comparing porosity of samples sintered at, 1000^{o}C, 1025^{o}C, 1050^{o}C, 1075^{o}C, 1100^{o}C, 1125^{o}C, 1150^{o}C, 1175^{o}C, or 1200^{o}C.

3.7 Scaffold characterization

Scanning electron microscopy (SEM) is used to measure actual particle size after attrition, pore size after sintering, rod dimension, surface morphology, and porosity. SEM samples need to be coated with a thin layer of gold. A piece of double sided carbon tape was placed on the surface of a metallic disc to electrically ground the sample. The sample is placed on the platform of a sputter coater (Cressington Q108 Auto). Air is evacuated

followed by an argon purge, and then a plasma flow containing ionized gold particles is used for duration of 10-15 seconds for coating the sample.

3.7.1 Porosity and density measurements

Porosity is assessed by Archimedes' method using the quantity of water retained in the meso and microporosity of the samples. First samples are weighed dry in air (M_o). The samples are boiled in de-ionized water for 1 hour. After cooling, samples are extracted from water with forceps and solid sides are blotted dry with paper wipes (Kimberly Klark professional wipes, Product 34256) and the weight is again measured (M_{wet}). The soaked samples are then measured immersed under water using a density kit (Product 225600, Mettler Toledo) to obtain the immersed weight (M_i). Soaked samples extracted are then blotted dry till no water stain can be seen on the paper wipe. Subsequently, compressed air (20psig, 10 SCFM) is blown through the ceramic samples for 5 seconds for each. Then a second wet weight is measured (M_{wet2}). The purpose of this air blowing step is to remove water from the macropore network of rods while retaining water in the microporosity of the rods. The Young-Laplace equation relates the capillary dimension(s) and surface tension to capillary pressure. In these measurements, the pressure used should be low enough only to expel water from the large (ca. >50µm) pores.

The total quantity of water absorbed by the sample (in large and small pores) is obtained subtracting the dry weight from the first wet weight, and the respective volume equals the total volume of pores in the sample. The quantity of water retained in the sample after blotting the samples dry is obtained by subtracting the dry weight from the

second wet weight, corresponds to the volume of micropores in the sample. Density is calculated following the equation:

$$\rho = \frac{M_o}{M_o - M_i}(\rho_{water} - \rho_{air}) + \rho_{air} \quad (3)$$

where, density of water (ρ_{water}) at the working temperature (22^oC) is known $0.9977 g/cm^3$ and the density of air (ρ_{air}) is also known $0.0012 g/cm^3$.

3.8. Soluble fillings

For the first type of samples, chitosan (Ch) gel 2.4% by weight concentration is used to fill the macro/micro pores of the ceramic scaffolds. An appropriate amount of Ch powder (Ultrason, Ultrapure Chitosan, Biosyntec, Canada, 70% deacetylated, 50,000MW) is dissolved in sterile deionized water at pH=6 in presence of acetic acid. Ceramic structures are immersed in the sterile chitosan gel in tissue culture hood then vibrated on a (Handler MFG, Westfield, NJ) vibrator for 2 minutes to help the material penetrate the scaffold. The excess gel is wiped off and samples are allowed to dry. The Ch-filled samples have an overabundance of viscous gel left on the surface to slowly penetrate thru capillary action. The specimens are left to air dry overnight, are sterilized in ethanol 70% solution in tissue culture hood, and then allowed to dry for another 24 hours under sterile conditions.

Other samples are filled with Baker CaS (J.T. Baker, Mallinckrodt Baker, Inc. Phillipsburg, NJ), an alpha hemi-hydrate that needs 0.3ml of water per gram of CaS to make a flowing paste. A little more, about 0.4ml, can be used if needed to make wet slurry. The CaS has at least 30 minutes of working time with distilled deionized water. CaS slurry is put in a small deep container, samples are immersed in slurry. The container with slurry and samples is shaken on the vibrator (Handler MFG, Westfield, NJ) for 2

minutes on highest power mode. The edges are scraped for excess material, and then samples are allowed to dry.

3.9 Dissolution studies

Two HA:βTCP mixtures are analyzed: high HA(60:40) and high βTCP (15:85) in three groups: empty (control samples), Ch filled, and CaS filled. Several types of architectures are studied. All samples are disk shaped, 11 mm in diameter and 3 mm in thickness. Disks have open mesoporosity on one of the flat sides and on the cylindrical side with one solid flat side. There are three groups with only uniform pore dimension: 250x250µm, 500x500µm, 250x500µm. Another group, quadrant shaped, has the volume of the disk split into four sections: two with square pores (one section with small square pores, the other section with large square pores) and two with long pores in the dimensions described earlier (see Table 2).

Table 2 Dissolution study sample dimensions and nomenclature

Sample type	Pore size (µm x µm)	Pore filler
250x250 E	250x250	Empty
250x250 CAS	250x250	Calcium sulfate
250x250 C	250x250	Chitosan
500x500 E	500x500	Empty
500x500 CAS	500x500	Calcium sulfate
500x500 C	500x500	Chitosan
250x500 E	250x500	Empty
250x500 CAS	250x500	Calcium sulfate
250x500 C	250x500	Chitosan
Q E	Quadrant	Empty
Q CAS	Quadrant	Calcium sulfate
Q C	Quadrant	Chitosan

Samples are immersed in 5ml simulated body fluid (SBF) each. Every 3 to 4 days samples are retrieved from the solution, blotted dry, and then weighed (AS214 Ohaus analytical balance, Fischer Scientific Co.). In order to obtain comparable results, the same amount of time and the same sequence of movements are dedicated to blotting every sample, using always fresh dry paper towels. Scaffolds are then immersed in fresh SBF solution.

SBF contains NaCl (8.053g/L), $NaHCO_3$ (0.353g/L), KCl (0.224g/L), K_2HPO_4 (0.174g/L), $MgCl_2 \cdot 6H_2O$ (0.305g/L), $CaCl_2$ (0.277g/L), Na_2SO_4 (0.071g/L), to which 5ml of Na_3N 2M solution acting as bacteriostatic is added per liter of aqueous solution. All these salts are added in 900 ml of sterile deionized water in a sterile 1000ml bottle. The solution is homogenized by agitating it until salts are dissolved. The pH of the solution is checked (pH meter Model 250 A+, Thermo Orion) and titrated to 7.2-7.4 by adding as necessary hydrochloric acid solution (0.1M) or sodium hydroxide solution (0.1M). The final quantity of water is added completing 1000 ml.

For the second dissolution study, quadrant-shaped samples printed using pure HA:βTCP=35:65 ink or HA:βTCP=35:65 blended with 15% starch ink or 25% starch ink are heat treated by sintering following the same program as beforehand prepared in two groups: empty and CaS filled. To assess the effect of sintering temperature on dissolution behavior, ceramic samples with HA:βTCP=60:40 are printed with 500x500µm pores (11mmØ, 3mm high, one solid flat side) and they sintered in the last step respectively at 1125^{o}C, 1150^{o}C, 1175^{o}C, and 1200^{o}C, for 4 hours. These samples were also prepared as empty and filled with CaS. Samples are immersed in 5ml simulated body fluid (SBF)

each. Every 3-4 days samples are retrieved from the solution, blotted dry, and then weighed (AS214 Ohaus analytical balance, Fischer Scientific Co.). Samples were grouped as can be seen in Table 3.

Table 3 Second dissolution study samples

Sample type	Pore size	Pore filler
HA:βTCP=35:65	Quadrant	Empty
HA:βTCP=35:65	Quadrant	CaS
15% rice starch, 85% HA:βTCP=35:65	Quadrant	Empty
15% rice starch, 85% HA:βTCP=35:65	Quadrant	CaS
25% rice starch, 75% HA:βTCP=35:65	Quadrant	Empty
25% rice starch, 75% HA:βTCP=35:65	Quadrant	CaS
1125 HA:βTCP=60:40	500x500µm	Empty
1125 HA:βTCP=60:40	500x500µm	CaS
1150 HA:βTCP=60:40	500x500µm	Empty
1150 HA:βTCP=60:40	500x500µm	CaS
1175 HA:βTCP=60:40	500x500µm	Empty
1175 HA:βTCP=60:40	500x500µm	CaS
1200 HA:βTCP=60:40	500x500µm	Empty
1200 HA:βTCP=60:40	500x500µm	CaS

3.9.1 Dissolution study data analysis

An initial dry weight of the scaffolds is registered, and then samples are immersed in SBF for 5-6 hours, blotted dry and weighed. This value is considered the initial wet weight that is taken in consideration as W_o. Data is expressed in weight at a certain moment in time divided by W_o ($W(t)/ W_o$) versus time in days. Absolute weight versus time (days) graphs are also generated.

CHAPTER 4

4.0 RESULTS AND DISCUSSION

The results of this study are presented following the order of the processing steps. Ceramic particles that are subjected to calcination and attrition milling are characterized in §4.1. As-printed structures before and after sintering are characterized in §4.2, to confirm that desired dimensions were obtained together with composition and architecture. *In vitro* dissolution studies results are presented in §4.3.

4.1 Powder Characterization

4.1.1 SEM characterization

Scanning electron microcroscopy was used to analyze approximate grain size of the powder before and after calcination and after attrition milling. The as-received and calcined HA powders are shown in the SEM micrograph of Figure 4. Large (Ø≥5µm) agglomerates are pervasive in the as-received powder. It is unclear what the primary particle size is in this state, however, the agglomerates appear to be porous and primary particles appear to be sub-micron in size. After calcination, the apparently porous aggregates are transformed into relatively smoother particles with particle size on the order of 2 to 5µm.

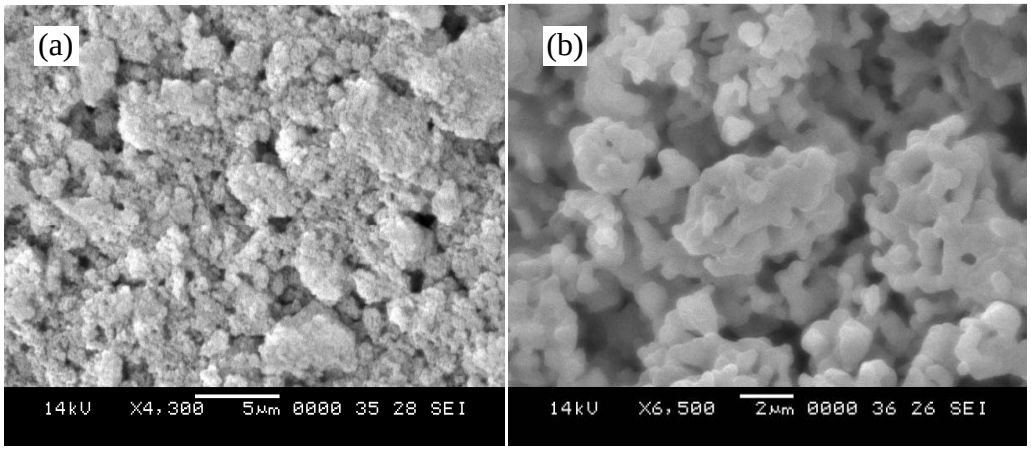

Figure 4 SEM micrograph of HA powder, (a) as-received, (b) calcined at 800^{o}C for 11 hours

βTCP powder can be seen in Figure 5 after calcination at 800^{o}C for 11 hours. The particles shown in the SEM micrograph appear to be smooth and fused into agglomerates of 5 to 10μm in diameter.

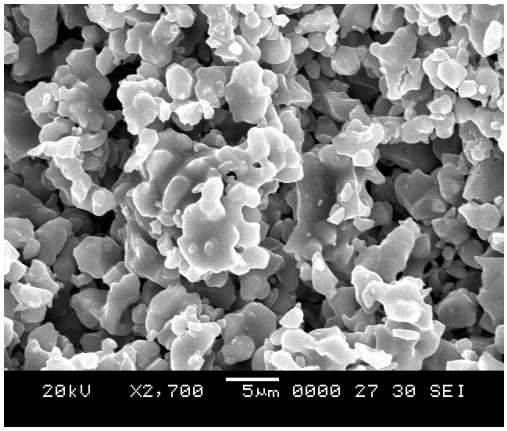

Figure 5 SEM micrograph of βTCP powder calcined at 800^{o}C for 11 hours

After attrition milling, the HA primary particle size decreases in proportion to milling duration and the mill speed (100%=500rpm). The morphology of the powder after attrition milling is more equiaxed and smaller in diameter compared to the calcined powder. In Fig. 6, there appears to be little difference between powders milled for 2.5h or

3.5h. In initial formulations, milling was performed for 3.5 h due to lack of knowledge of particle size as a function of milling time. The time of 3.5 h was chosen as a "safe" time to achieve particle size reduction. The morphology of the ceramic powder influences the performance of the resulting ink, as demonstrated by Miranda *et al*., [23].

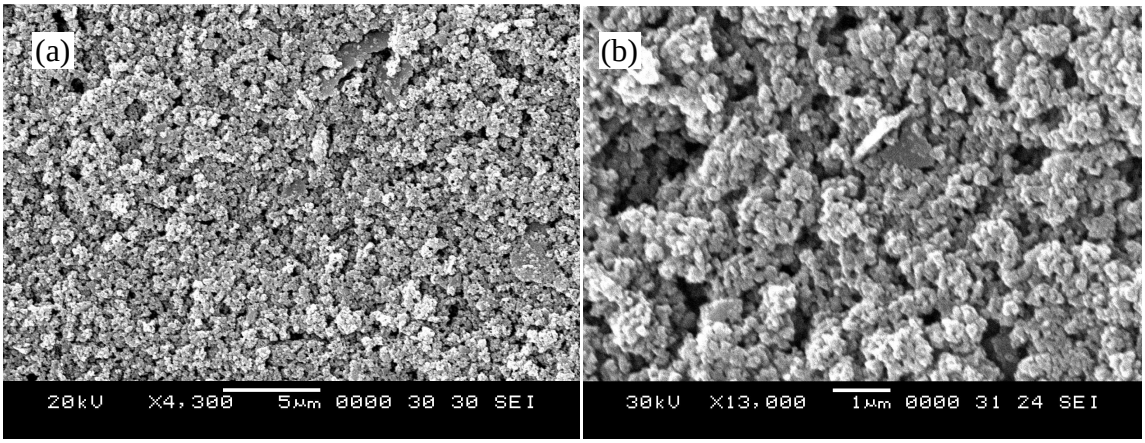

Figure 6 SEM micrographs of HA powder after (a) 2.5 h attrition milling and (b) 3.5 h attrition milling.

4.1.2 X-ray diffraction of the ceramic powder

X-ray diffraction Cu-kα radiation is used to assess the crystallinity of the powder before and after calcination. Figure 7 shows the superimposed diffraction patterns for calcined and as-received HA. The calcined HA displays well-defined sharp peaks at 2θ angles expected. The as-received HA displays peaks at appropriate 2θ values, however, these peaks are broad indicating either a significant amorphous component or, more likely, peak broadening due to nano-crystallite size.

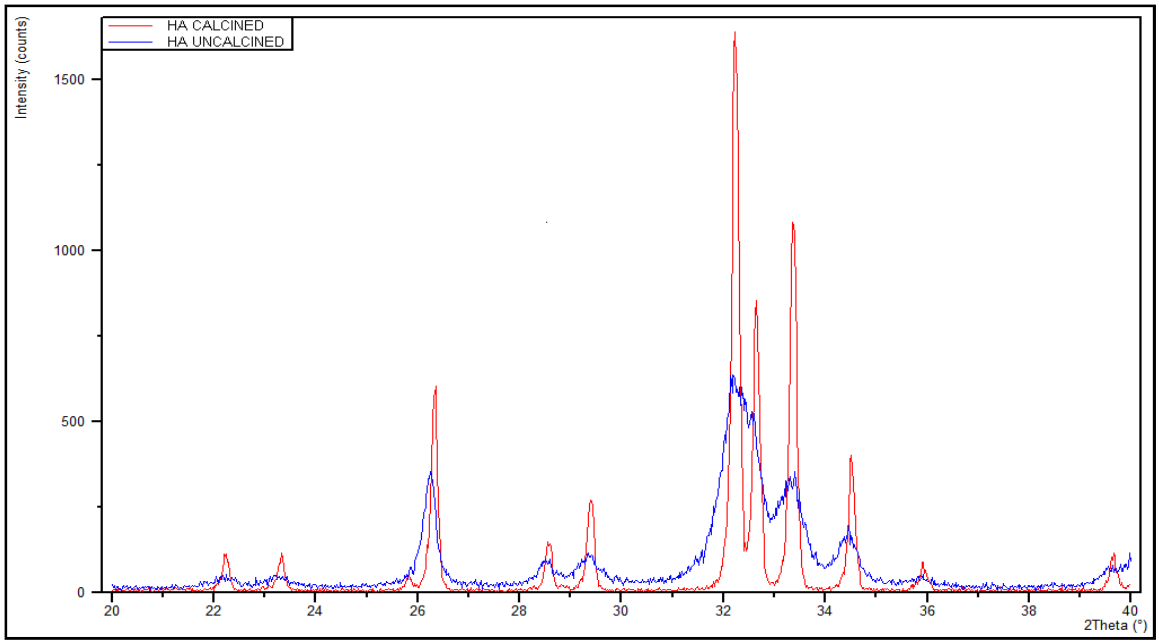

Figure 7 XRD of uncalcined (blue line) and calcined (red line) HA powder

The diffraction patterns for βTCP before and after calcination indicate that the as-received powder is highly crystalline. The 2θ shift in diffraction peaks for the calcined powder indicates a contraction of the lattice parameter associated with dehydration of the powder, [64].

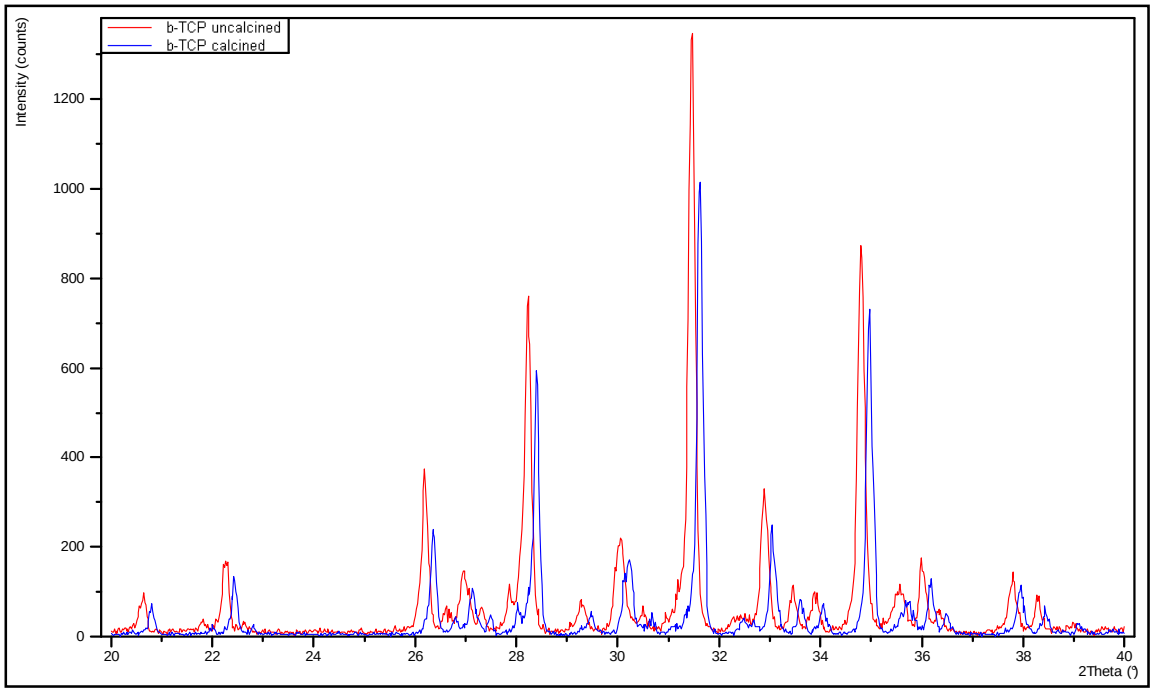

Figure 8 XRD of uncalcined and calcined βTCP powder

The HA:βTCP mixtures after sintering display X-Ray diffraction peaks characteristic for both HA and βTCP, as shown in Figure 9. Specifically, the peaks at 2θ = 23.3°, 28.7°, 32.2°, 32.8°, 34.5°, and 39.8° are indicative of the HA component. In the HA60TCP40 pattern, these peaks are obviously present along with a number of peaks specific to βTCP. For the HA15TCP85, the HA specific peaks are muted due to the lack of volume of HA present. It is unclear if the HA phase is transformed to βTCP, however this is unlikely due to the stoichiometry and processing temperature. Rather, it is likely that the intensity of HA peaks is masked by those for the βTCP.

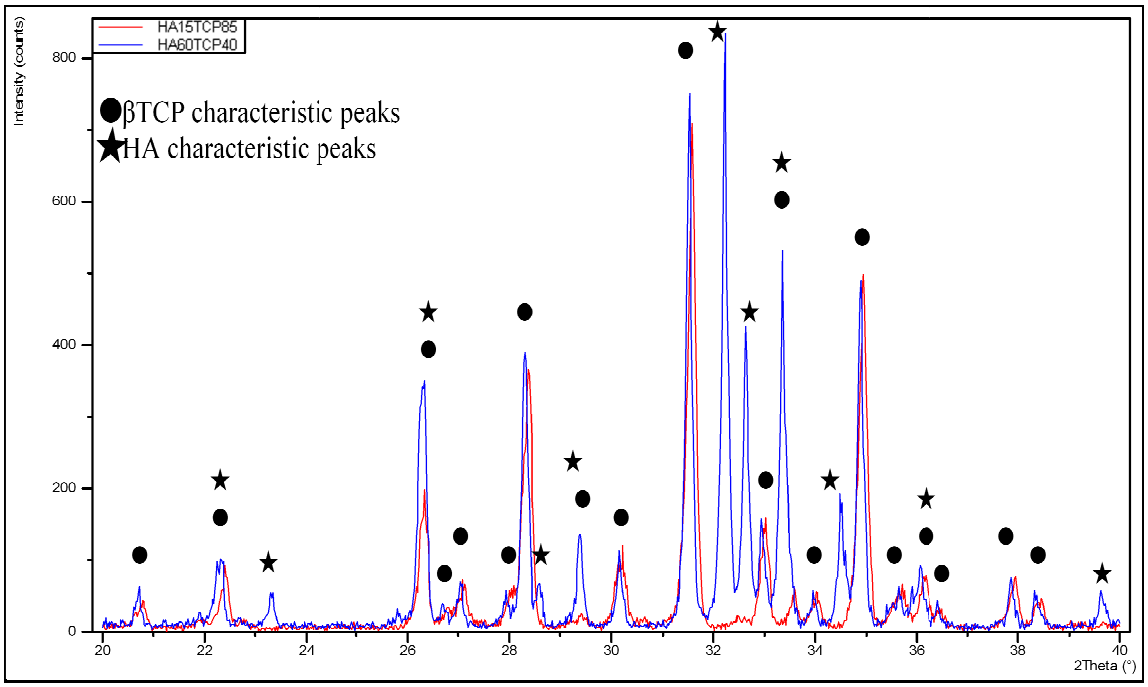

Figure 9 XRD patterns for the two mixtures of HA and TCP: HA15TCP85 (red line) has 15% HA, HA60TCP40 (blue line) has 60% HA; characteristic peaks HA (stars), TCP (disks)

4.1.3 Particle size analysis

Particle size was analyzed using an acoustic spectrometer (Model DT-1200, Dispersion Technology Inc.). For HA, the particle size distribution can be seen in Figure 10, after 4 hours of attrition milling. The average particle diameter is $<\text{Ø}>=0.56\mu m$ and the distribution has a standard deviation of $\sigma=0.03\mu m$.

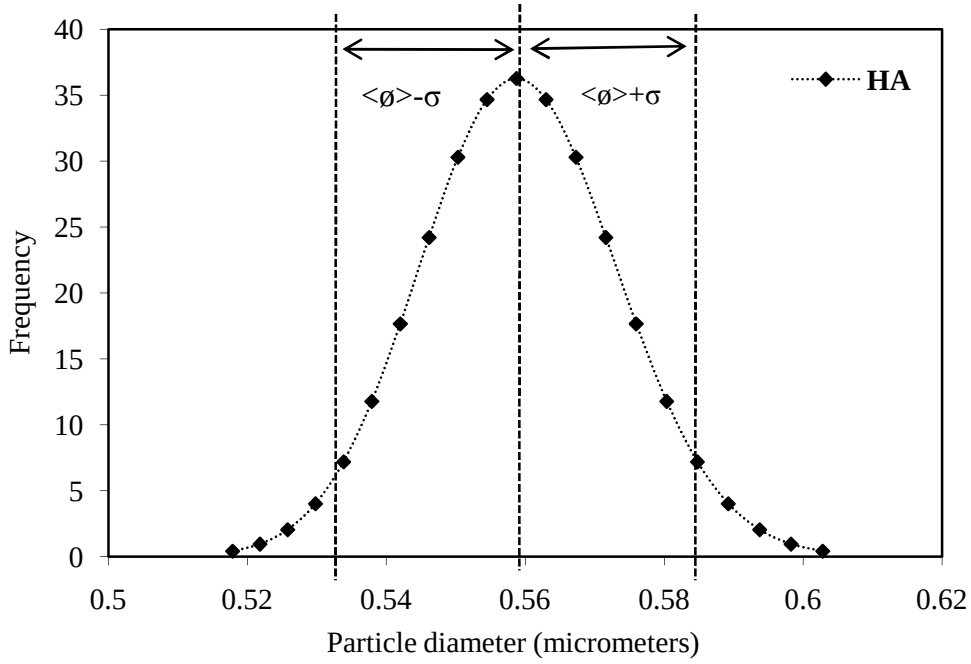

Figure 10 Particle size distribution for HA after milling for 3.5 hours

In a complimentary experiment to assess the efficiency of the milling, dynamic light scattering (DLS) was performed on small samples retrieved from the milling charge as a function of milling time. DLS was chosen due to the small sample size required (1mL). Average particle diameter is graphed as a function of milling time in Figure 11. Initial average particle size is 3.85µm for HA and 4.12µm for βTCP. The particle size decreases abruptly in the first 15 minutes of milling to 2.07µm for HA and 1.13µm for βTCP. Both materials are reduced to particle size less than 1µm after 75 minutes of milling. HA continues to remain at about 0.7µm range for about 2.5 h then drops to 0.462µm after five hours of grinding. βTCP reaches the 0.4µm average particle size value after 2.25 h of milling.

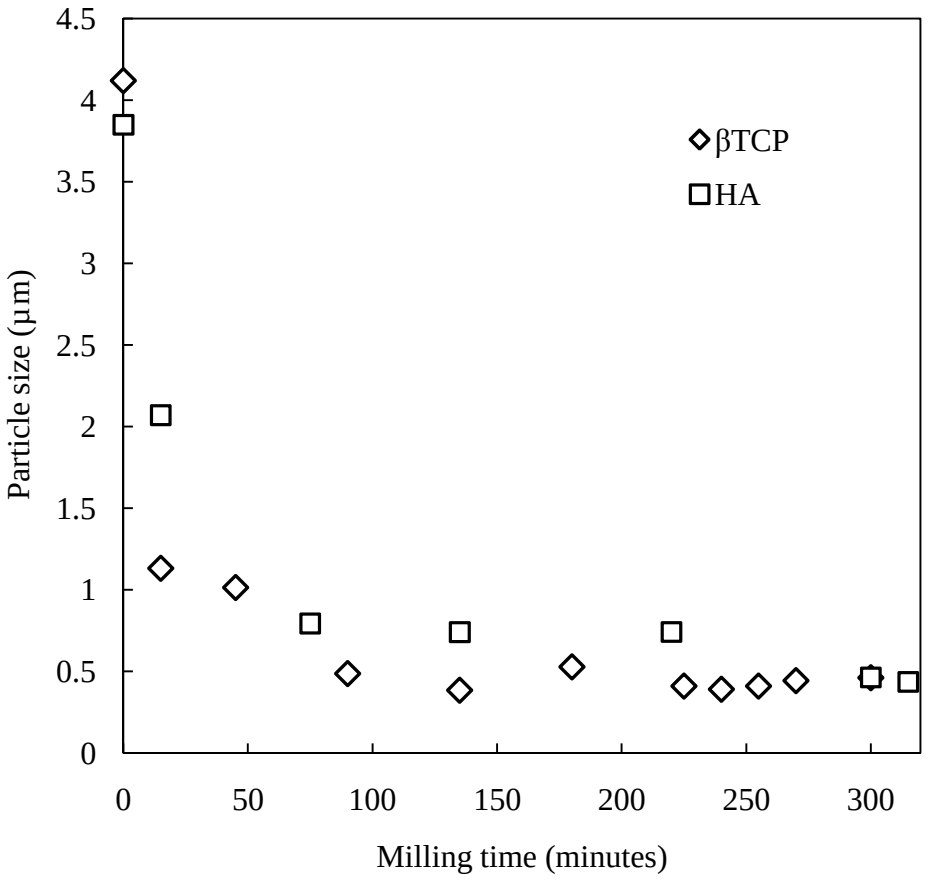

Figure 11 Average particle diameter as a function of milling time for βTCP (diamonds) and HA (squares) as measured by DLS

4.2 Characterization of the printed samples

4.2.1 Pure HA:βTCP Scaffolds

To characterize the macroscopic lattice spacing (i.e., pore size) of the printed and sintered structures, scanning electron microscopy was used to capture images and a ruler was used to measure the pore size relative to the SEM scalebar. Figure 12 M1 below shows the 3D model of the quadrant structure and a top view of the same structure model

in Figure 12 M2. The lateral view (Figure 12A) obtained via optical microscopy was used to verify the open porosity on the lateral surface of the samples. The center of a quadrant structure was visualized under SEM for a precise measurement of the mesopores. Pores are measured rod surface to rod surface. Pore sizes measured this way are: 250x250µm, 250x500µm, 500x500µm, and 250x500µm. Multiple measurements (5) were performed for each dimension and then results were averaged with an approximate precision of ±10µm.

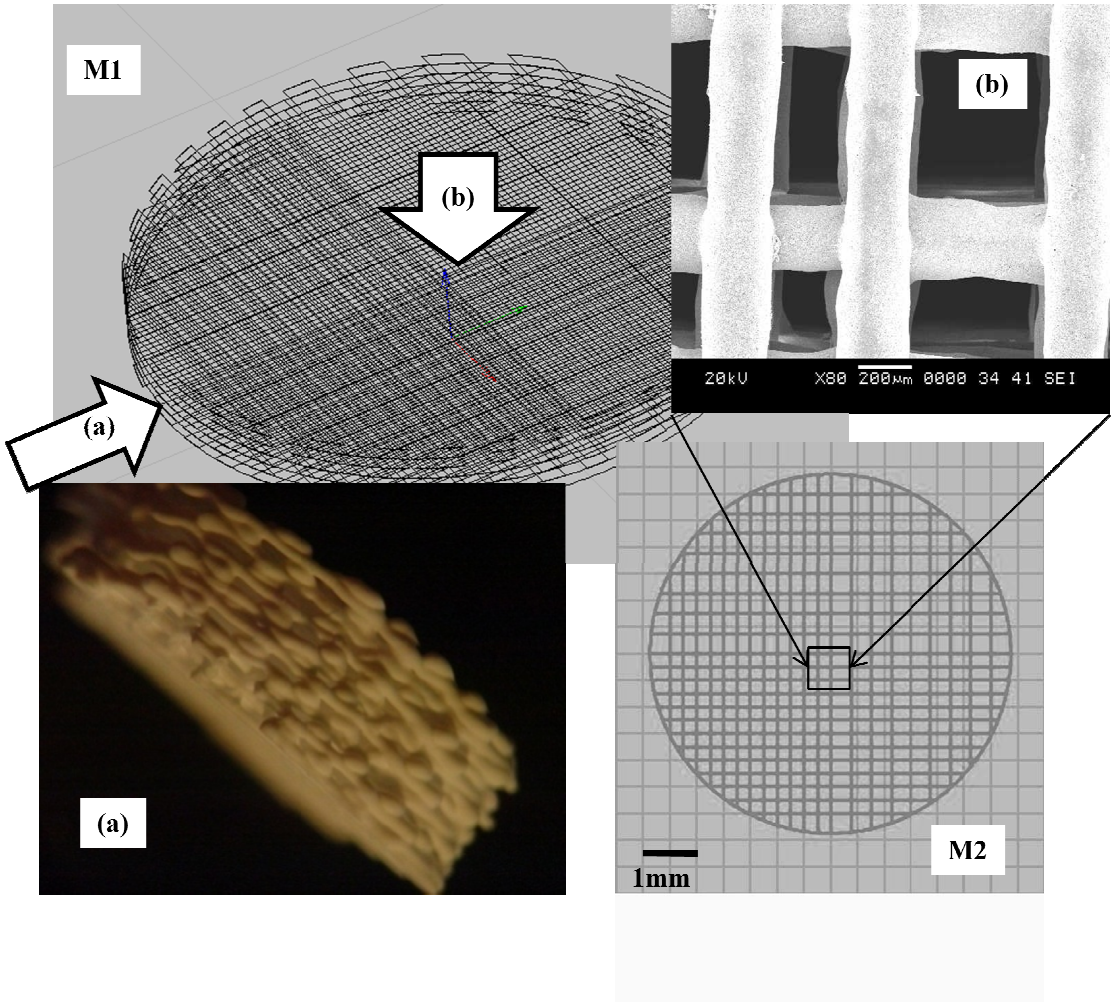

Figure 12 M1: Graphic 3D model of the quadrant structure. M2: Top view of the model. (a): Photograph of the lateral view using optical microscopy (4X). (b): SEM micrograph of the center of the quadrant structure for mesopore measurement

The printing process and the design of the scaffolds followed that used in Simon *et al*. study, [62]. The size and dimensions of the studied samples (11mm diameter, 3mm high, and one flat side solid) copied the size and dimensions of the parietal trephine defects, which is one of the standard models for *in vivo* trials of bone scaffolds.

4.2.2 Fugitive Starch Ink Blended with HA:βTCP for Added Micro-Porosity

Fugitive rice starch ink was printed and heat treaded in volumetric ratios of starch:ceramic of 15:85, 25:75 and 50:50. The sintered ceramic structures in Figure 12 show the increase in porosity and average pore size with increasing starch content. The pore diameter is approximately 1µm for the ϕ_{starch}=0.15 mixture (B), while at ϕ_{starch}=0.25 the pores reach ≈5µm in diameter (C). The ϕ_{starch}=0.50 mixture shows a very open ceramic structure.

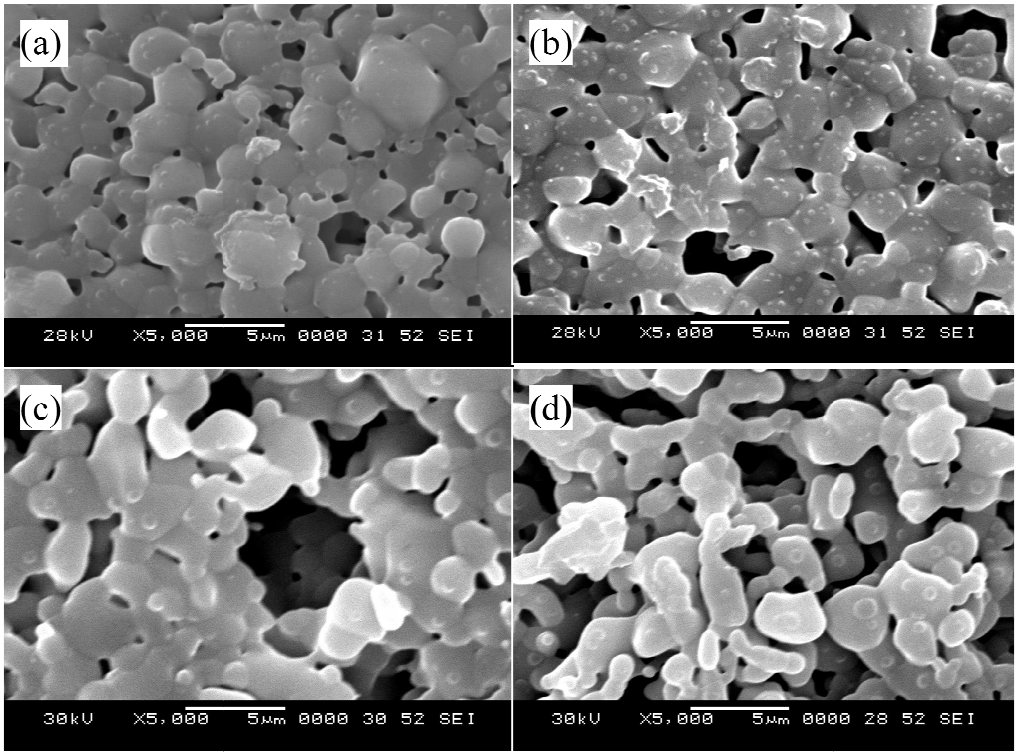

Figure 13 SEM micrographs for surface assessment of rice starch and HA:βTCP mixtures after sintering: (a) ceramic only, ϕ_{starch}=Vstarch/(V_{starch}+$V_{ceramic}$) (b)=0.15, (c) = 0.25 , (d) = 0.50

4.2.3 Sintering Shrinkage and Porosity in Pure HA:βTCP Scaffolds

Sintering shrinkage is assessed by diametrical and thickness measurements of disk shaped samples as a function of sintering temperature. Figure 14 shows samples fabricated from HA:βTCP=60:40 at initial diameter of 10mm and then fired for 4 hours at different temperatures 1100, 1125, 1150, 1175, and 1200 ^{o}C. As the photograph illustrates, sintering shrinkage scales in proportion to sintering temperature with the1200^{o}C sample shrinking more than the one fired at 1100^{o}C.

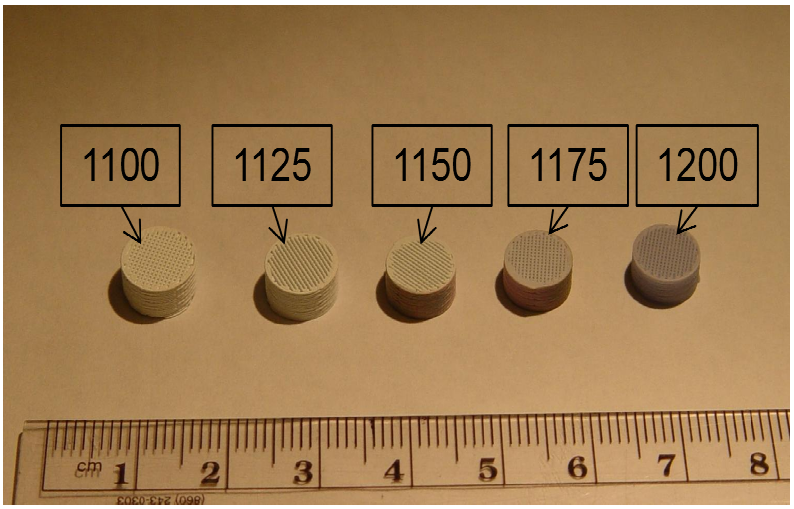

Figure 14 Photograph of HA:βTCP=60:40 samples for shrinkage assessment printed at same dimensions and fired at different temperatures (as labels indicate) for 4 hours

The percent change in diameter of the samples is measured and plotted in Figure 15 as a function of sintering temperature. The maximum linear shrinkage for sintering can be estimated from knowledge of the ceramic volume in the green body and assuming 100% densification. Assuming a cube of material with initial side length l_o and green body solid volume fraction of ϕ_o, the percent linear shrinkage (%LS) is calculated by:

$$\%LS = \left(1 - \left[\frac{\phi_o}{\phi_f}\right]^{\frac{1}{3}}\right) \cdot 100\%$$

where ϕ_f is the solids volume fraction after sintering. If $\phi_o = 0.47$ and $\phi_f = 1.0$, $\%LS = 22.2\%$.

Porosity is determined by the Archimedes's method. The theoretical density of the composite scaffold HA:βTCP=15:85 is 3.09 g/cm^3 based on a volume fraction weighted average of the HA and βTCP densities of 3.02 g/cm^3 and 3.11 g/cm^3, respectively. As expected, the density of the ceramic scaffold increased asymptotically toward 3.11 g/cm^3

at a sintering temperature of 1200^{o}C as illustrated in Figure 18 (within experimental error). The Archimedes density measurement agrees with the porosity trend observed in Figure 17 the amount of micro-porosity in the scaffold rods decreases as sintering temperature increases. Micro-porosity decreases from 23.52% in the rods at 1100^{o}C to 8.32% at 1125^{o}C and disappears entirely at 1200^{o}C. A parallel trend is followed by the total porosity while the meso-porosity remained relatively constant from 28.23% to 22.85% (within error limits).

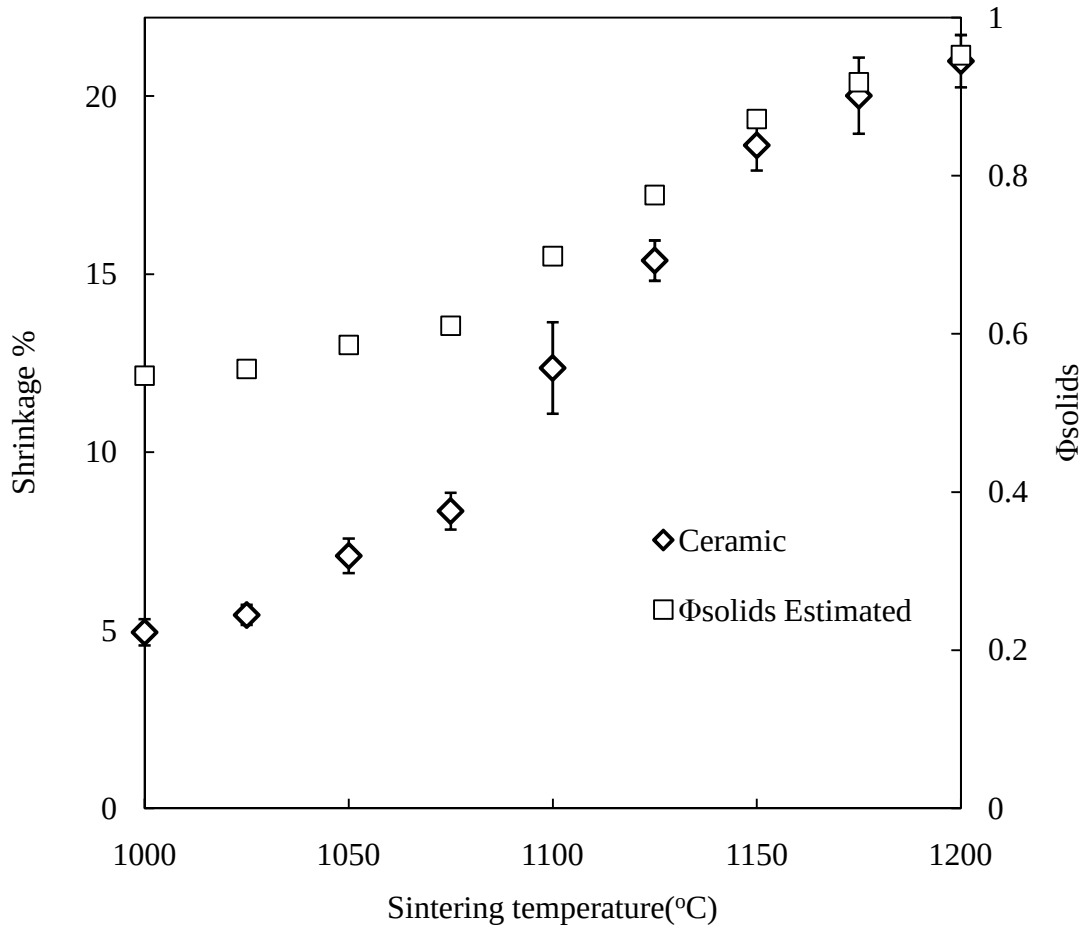

Figure 15 Linear shrinkage of samples sintered for 4 hours at different temperatures

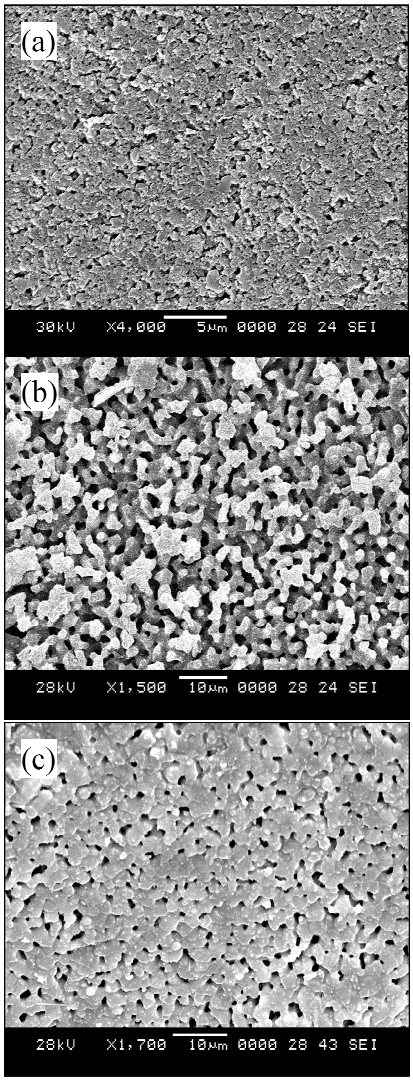

Figure 16 SEM micrograph for assessment of (a) green body surface, (b) ceramic surface after sintering at 1100^{o}C for 2 hours, (c) ceramic surface sintered for 4 hours at 1100^{o}C

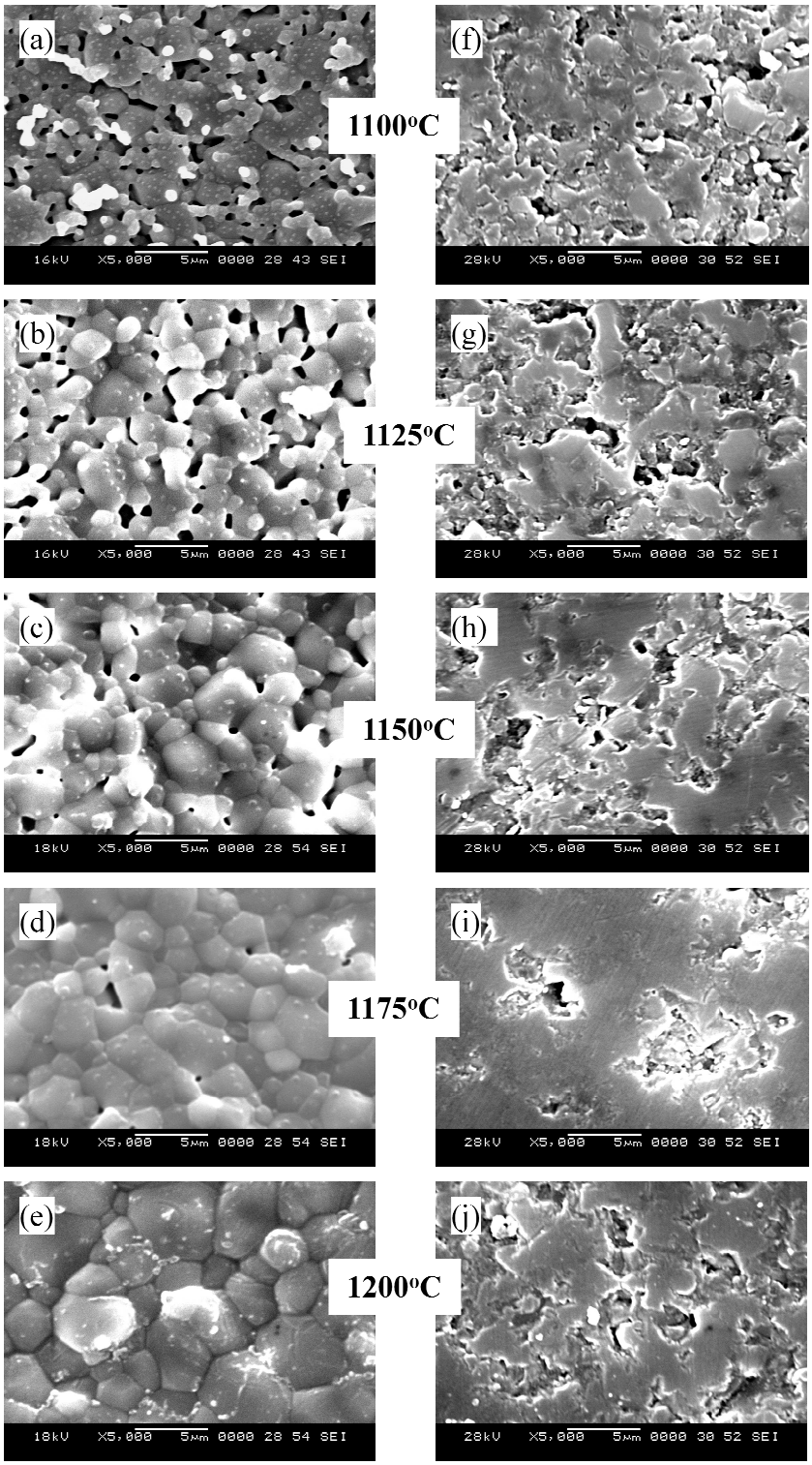

Figure 17 SEM micrographs of surface (a) to (e) right and sections (f)-(j) for HA:βTCP=60:40 sintered at different temperatures (as labels indicate) for 4 hours

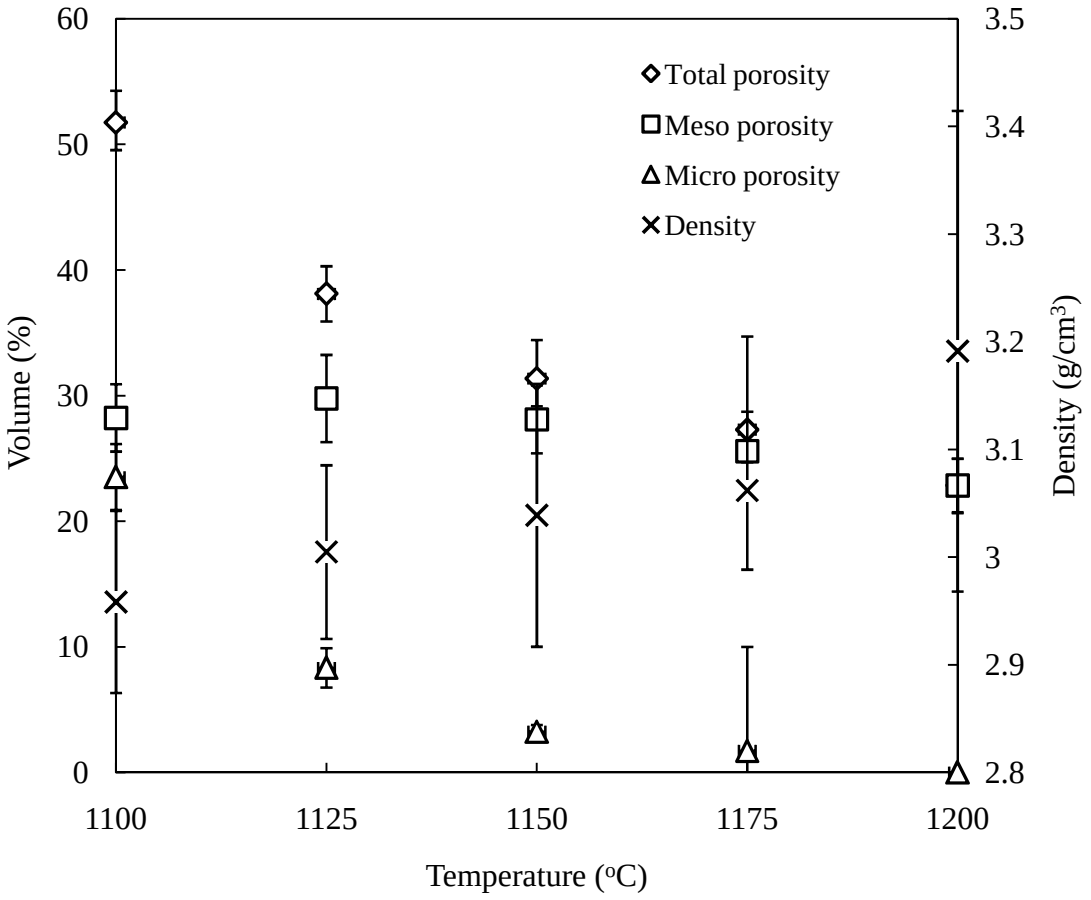

Figure 18 Graph showing evolution of percentage of volume occupied by various types of porosity (total porosity-diamonds, meso porosity-squares, micro porosity-triangles) versus the sintering temperature. On the secondary axis: the evolution of density versus the sintering temperature

A similar study by Yang *et al.* in 2008, [65] analyzes porosity/ densification of HA:βTCP mixture-based ceramics obtained by extrusion sintered at 1100, 1150, 1200, 1250 and 1300^{o}C for four mixtures of HA and βTCP, containing HA in 100, 75, 50 and 25 %. The 60% HA mixture that made the object of the current study of porosity/density

variation with sintering temperature (see page 46) shows a density of 2.96g/cm^3 corresponding to 1100^{o}C sintering, much larger than the value of 1.98g/cm^3 that Yang *et al.* obtain for the same temperature treatment, 50% HA mix.

The likely difference lies in the method of obtaining density. In the Yang case, bulk dimensions and weight of the samples are used to calculate density. This method counts open porosity in the density measurement. In the Archimedes method, the open porosity is filled with water and the density measurement only includes porosity closed to water penetration. The current data suggests that for the 2.96 g/cm^3 sample that should have a density of 3.11 g/cm^3 if no porosity exists in the rods has a volume fraction of closed porosity equal to $\phi_{closed\ pore}$=0.048. In this sample, the total microporosity was calculated to be $\phi_{microporosity}$=0.24. Hence, most of the microporosity is open and it is expected that bone cells interfacing with this scaffold may be able to communicate by canaliculi extension through this open micropore network.

4.3 Dissolution study results

4.3.1 Pure HA:βTCP Scaffold

The absolute mass evolution in time of the three groups of samples: empty (E), Calcium sulfate filled (CaS), and Chitosan filled (C), can be seen in the Figure 19.

(a)

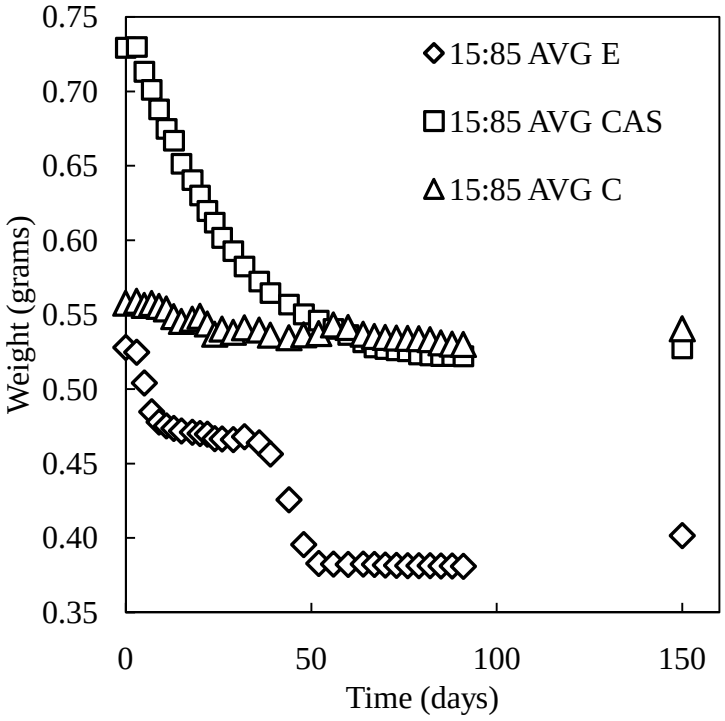

(b)

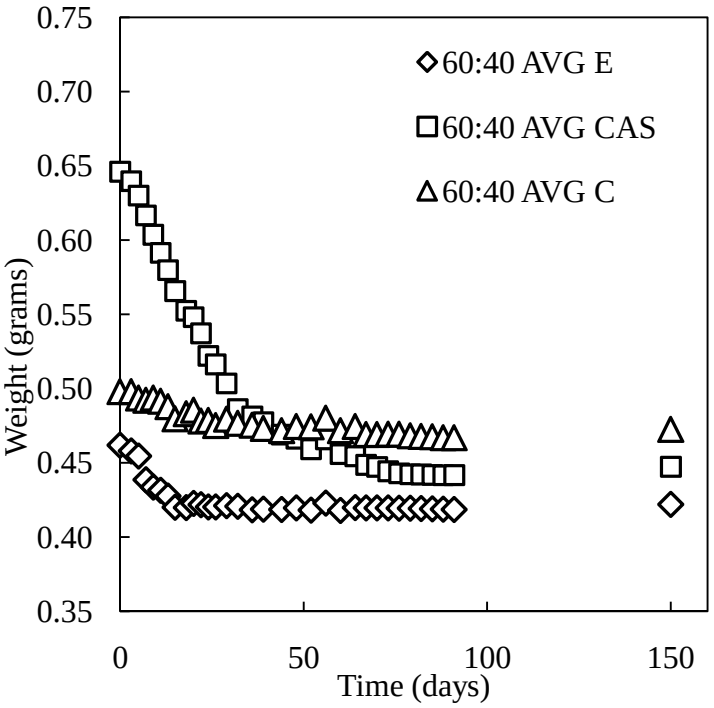

Figure 19 Graphs showing evolution of absolute mass of the samples in time (a) HA:βTCP=15:85, (b) HA:βTCP=60:40

The initial mass of the samples differs as a function of the existence of filler and filler type: CaS filled samples have an extra 200mg of filler compared to the empty samples, while C filled samples have only an extra 50mg compared to the same empty samples. Initial mass of the empty samples in the high HA mixture is smaller than the high βTCP mixture because of βTCP's higher density.

HA:βTCP=60:40 empty samples lost about 9% of their weight within the first 15 days, and then stabilized. In comparison, HA:βTCP=15:85 empty samples showed similar weight loss over the initial 10 day period followed by an abrupt drop in weight of approximately 14% around day 40 to 50, after which they finally stabilized. The second step change in weight is likely due to lost material during the weighing process since the samples became extremely delicate at this point. A small accumulation of fine powder material, assumed to be the result of spalling, was noticed at the bottom of the test tube, material which was not possible to be exactly quantified since it passed through the mesh used for sample transfer during solution change operation.

Both types of mixtures when filled with CaS demonstrate a monotonous weight loss from day 1 to day 75. Note, the terminal weight of the CaS filled scaffolds was approximately equal to the initial weight of a comparable empty scaffold and the terminal weight of initially empty scaffolds after dissolution was significantly less. The C filled steadily lost about 5% of their initial weight for the HA:βTCP=60:40 case and about 2.5% for the HA:βTCP=15:85 case.

The relative weight evolution of CaS filled HA:βTCP=60:40 scaffolds with a variety of pore dimensions are shown in Figure 20. Large square pore samples

(500/500CAS) lost the largest relative amount of weight (38.1%) while the small square pore samples (250/250CAS, squares in Figure 20) show a smaller relative weight loss of about 20%. The long pore samples (500/250CAS) and the quadrant (Q CAS) shaped ones demonstrate an average between the two extremes with a 22% mass loss.

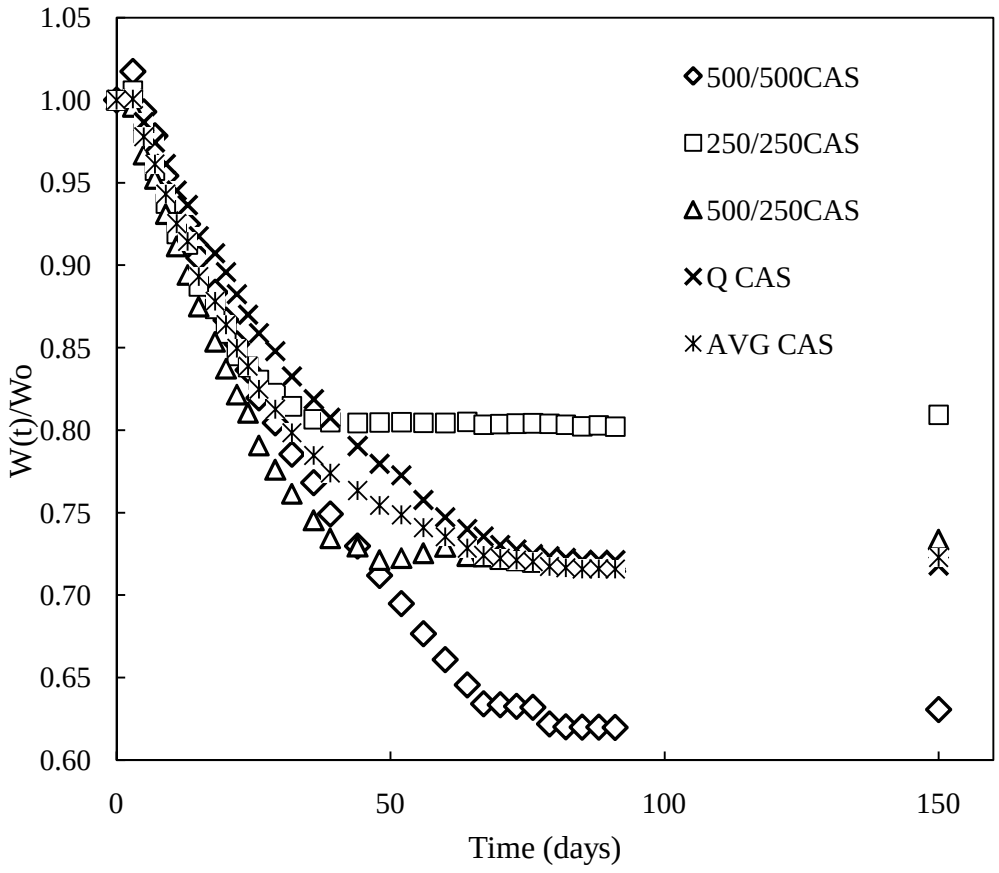

Figure 20 Graph showing dissolution of HA:βTCP=15:85, CaS filled samples

An SEM micrograph of a CaS-filled sample retrieved from the SBF after 54 days is shown in Figure 21. The section was obtained by embedding the sample in epoxy and then slicing with a diamond saw (EXTEC Labcut 1010, Extec Corp.). A residue of the CaS filling can be observed in the middle of the image (lighter grey lenticular shaped).

The upper side of the structure is free of any filler; rods are embedded directly in epoxy resin, as well as the sides of the structure, from where the filling has dissolved. Near the solid face of the disk sample (bottom in Figure 21), the CaS shows minimal dissolution as expected given the limited exposure to the SBF.

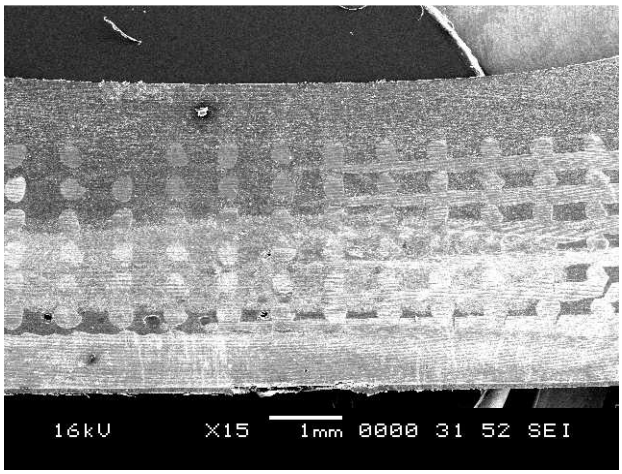

Figure 21 SEM micrograph of a section of a high TCP, CaS filled structure after 54 days in SBF

The empty sample (HA:βTCP=60:40) seen in Figure 22 was retrieved from SBF after 54 days. It shows signs of surface erosion. Spalling of the surface can be observed. A rather large chip with a fracture of approximately 50µm long can be observed as well as another larger piece.

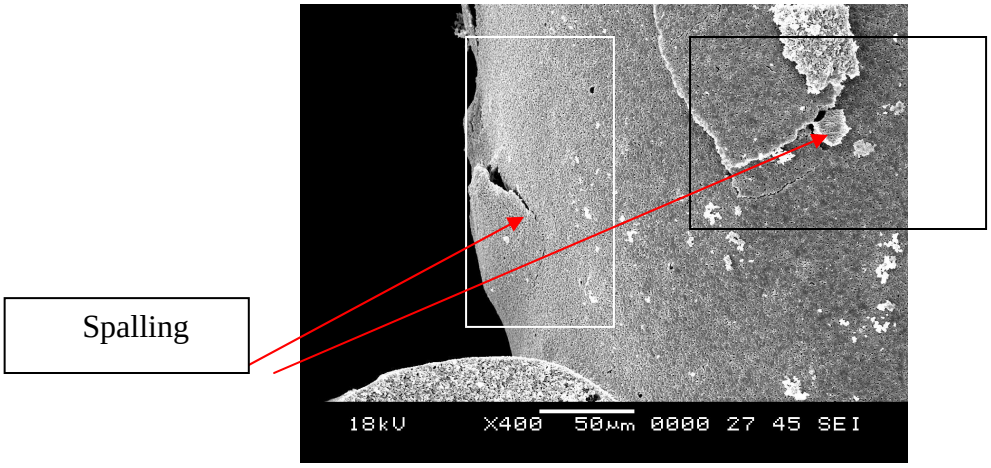

Figure 22 SEM micrograph of **HA:βTCP=60:40** empty structure after 54 days in SBF

At day 90, the daily SBF solution change was terminated. The samples were extracted from the solution on day 150, washed in plenty of deionized water, then denaturated ethanol, and allowed to dry. SEM micrographs were taken to visualize the surface of the samples and rod cross sections. Figure 23 is a micrograph of the surface of a HA:βTCP=15:85 empty structure. Enlarged micropores and some spalling caused by erosion can be observed. Same spalling can be blamed for the massive mass loss of the 15:85 empty samples in the first dissolution study.

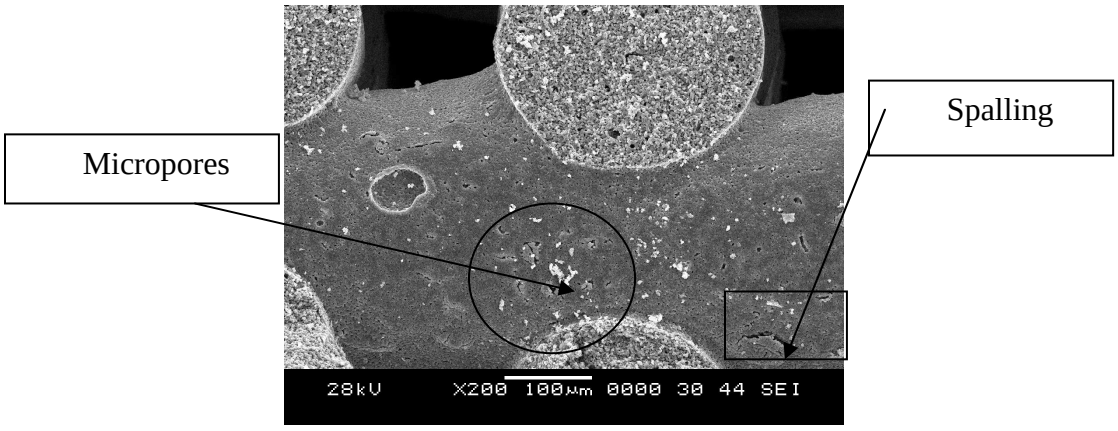

Figure 23 SEM micrograph of HA:βTCP=15:85 empty structure after 150 days of dissolution in SBF

For comparison, Figure 24 shows the surface of a HA:βTCP=60:40mixture, after 150 days of dissolution. The surface appears much smoother, showing less wear, which was expected since the HA is less soluble.

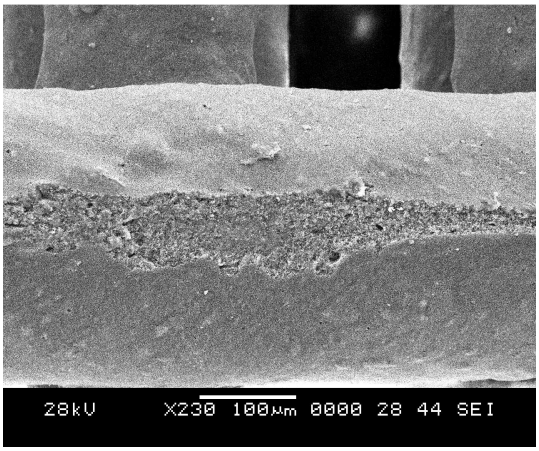

Figure 24 SEM micrograph of HA:βTCP=60:40 empty structure after 150 days in SBF

In the second dissolution study the behavior of HA:βTCP=35:65 mixture was observed in time. Figure 25 shows the weight evolution of these samples together with the corresponding empty samples made out of the other two mixtures: 15:85 and 60:40, which were analyzed in the first dissolution study. The evolution of the three types of samples remains parallel until day 40 when the 15:85 mix shows a rapid drop in weight of 73.6mg in 14 days. All samples have their evolution stabilized by day 60 of the study.

These studies served as control data for a parallel *in vivo* study at the Ney York University, Department of Biomaterials and Biomimetics. The parietal trephine defect is used for assessing properties for bone scaffolds for non-load bearing implants, however, these scaffolds may also prove useful for long bone scaffolding where mechanical stress is present during healing. Miranda *et al*. present in their study, [66], the mechanical properties of the scaffolds printed out of HA and βTCP. According to their results, HA-

fabricated scaffolds are mechanically superior to βTCP-made ones and would be better suited for load bearing conditions, demonstrating even better qualities after immersion in SBF. This observation is consistent with what we observed during our dissolution experiments: samples made out of high HA mixtures showed less dissolution/erosion compared to ones with high βTCP concentration.

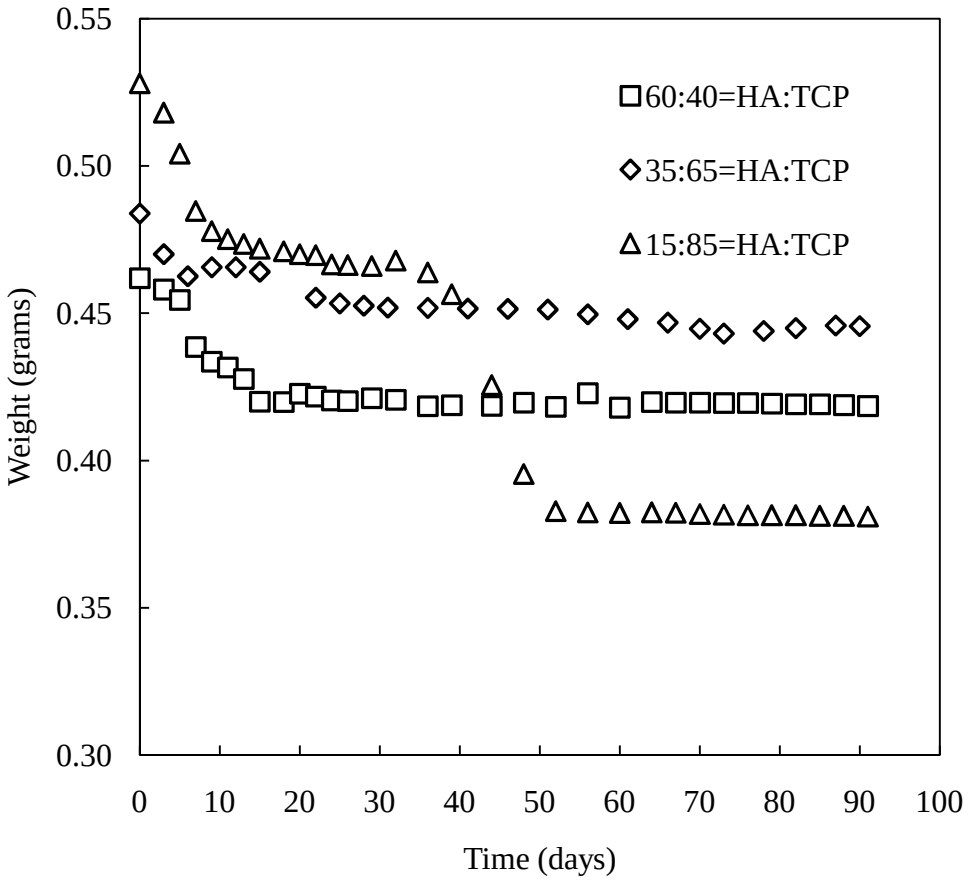

Figure 25 Weight evolution for empty 15:85, 60:40, and 35:65 mixture

4.3.2 HA:βTCP with Fugitive Phase

The weight evolution of fugitive ink, HA:βTCP ink mixtures, is shown in Figure 26. The ceramic samples prepared with rice starch lose less of their weight than the pure ceramic (*i.e.*, 0% rice starch). The 25% rice starch mix loses only 0.48% of its weight after 6 days, while the 15% rice starch mix loses 1.48% in the same time. In comparison, the pure ceramic samples loose 4.38% of their weight in the first 6 days. The rice starch mix samples stabilize their weight by day 30 of the study, while the ceramic samples stabilize around day 30 until day 52 with another decrease in mass in the period between day 52 and 75.

Interestingly, the weight of the starch mix samples appears to gradually increase over time beyond about 20 days. The likely mechanism for this weight gain is the precipitation and growth of bio-apatite crystals on the surface of the underlying HA:βTCP scaffold. With the increased microporosity of the starch mix samples, the microenvironment for precipitation is enhanced due to a greater availability of Ca^{2+} supplied by the higher specific surface area material. Once a layer of bio-apatite forms, it is stable in SBF and this could explain the minimal weight loss in the starch mix samples despite the increased specific surface area. The phenomenon of precipitation of bioapatite was also observed by Miranda *et al.*, [66]. The bio-apatite precipitated is a phosphate that has Calcium partially substituted by other ions like: Magnesium, Sodium and Potassium.

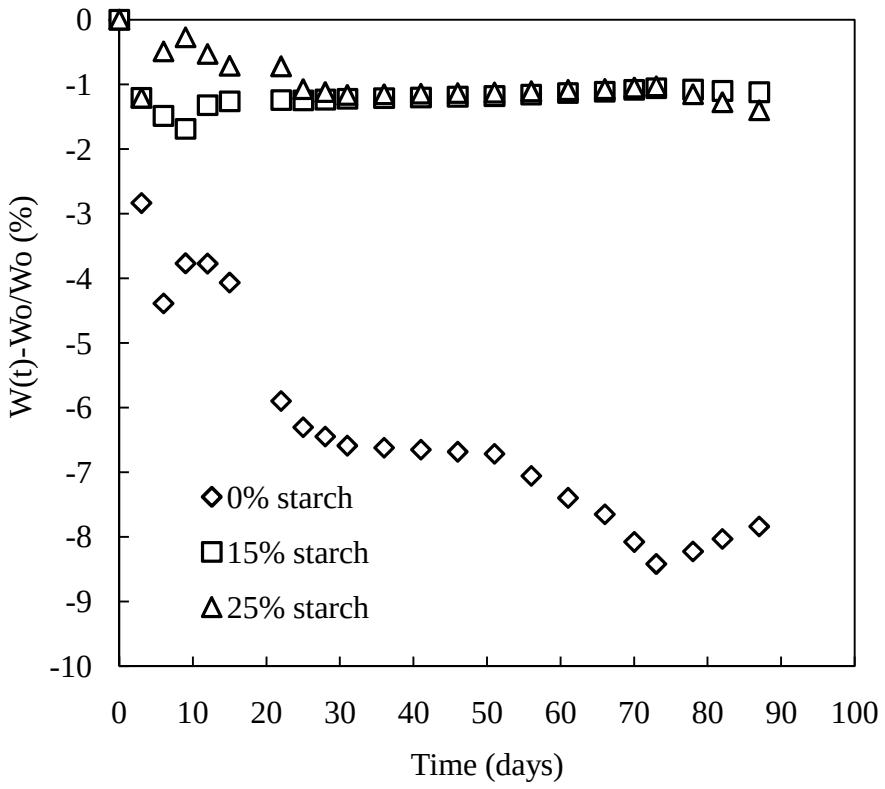

Figure 26 Weight evolution of ceramic samples of HA:βTCP=35:65, 85% HA:βTCP=35:65 and 15% starch, and 75% HA:βTCP=35:65 and 25% starch

To understand the bioapatite precipitation phenomenon within the ceramic-starch mixed samples, a 10-days experiment was performed. In this experiment, 25% rice starch samples were immersed in simulated body fluid and retrieved from solution, respectively, at 5 days, and 10 days. These analyzed in the SEM equipped with an x-ray microprobe (Hitachi electron microscope, model S-3500N and Princeton Gamma Tech IMIX x-ray microprobe system with a PRISM light element detector). Figure 27 shows an overview image of a sample retrieved after 5 and 10 days in simulated body fluid. Evidence of precipitate is present at grain boundaries within the pore structure. The 5 day specimen

shows some precipitate in the micropores of the ceramic (see Figure 27 (a)). There is more precipitate in the day 10 specimen (Figure 27 (b)) appearing as small clusters of particles.

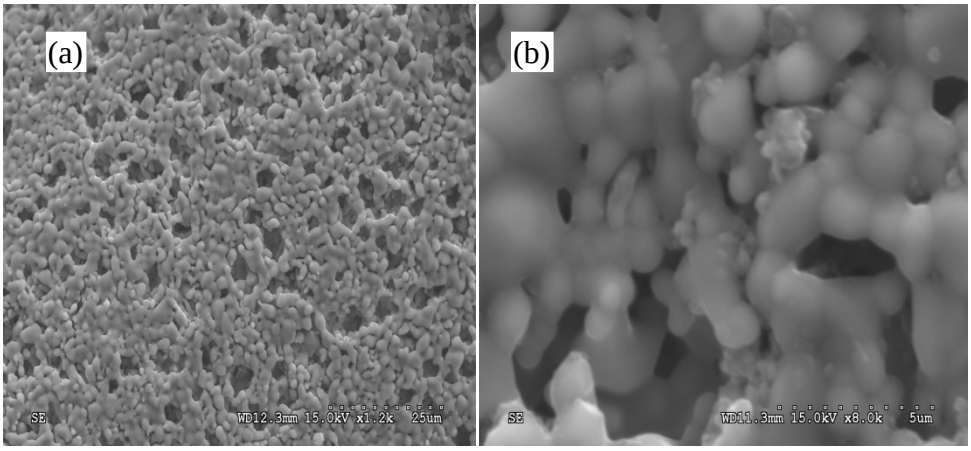

Figure 27 SEM micrograph of the sample immersed in SBF for 5 days (a) and 10 days(b)

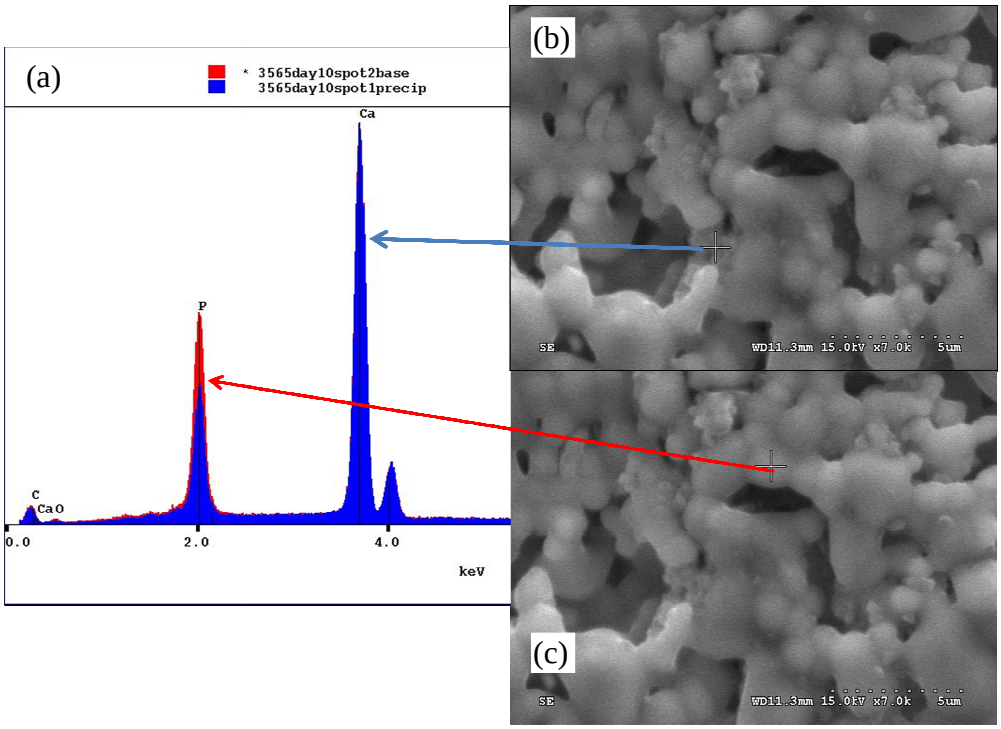

Figure 28 (a) X-ray microprobe spectra of the substrate material (red) and precipitate (blue); (b) and (c) SEM micrograph of the sample immersed in SBF for 10 days, hairpins and arrows indicate locations where spectra were taken

The x-ray microprobe analysis is shown in Figure 28. The SEM images highlight the points of microprobe analysis for the precipitate (b) and the base material (c). This precipitate displays a higher calcium/phosphorus ratio than the scaffold itself and appears to be hydroxyapatite rather than HA/TCP. There is more phosphate (P) in the base (HA/βTCP, lower Ca/P ratio) than in the precipitate (HA only, higher Ca/P ratio). Thus, the precipitate is probably HA.

4.3.3 Effect of Sintering Temperature on Dissolution Behavior

Sintering temperature has been shown to affect the density of the HA:βTCP samples, with higher temperature resulting in higher density. The higher density implies a lower total surface area as the amount of open microporosity decreases. In such a case, one would expect that chemically similar samples sintered at different temperatures would show different dissolution kinetics.

As can be seen in Figure 29, samples that were treated at higher temperature lost less mass relative to their initial weight than the ones treated at lower temperature. After 9 days, the samples sintered at 1100^{o}C lost 8.15% of their mass, while the ones sintered at 1200^{o}C lost only 1.68%. The samples treated at intermediate temperatures lost in the first 9 days, respectively, 4.88% (1125^{o}C), 2.23% (1150^{o}C), and 1.61% (1175^{o}C). All samples demonstrate a slow increase in weight after day 60 of the study due to precipitation of salts from simulated body fluid. The samples that were sintered at 1175^{o}C recuperate the weight initially lost and after day 85 surpass the original weight.

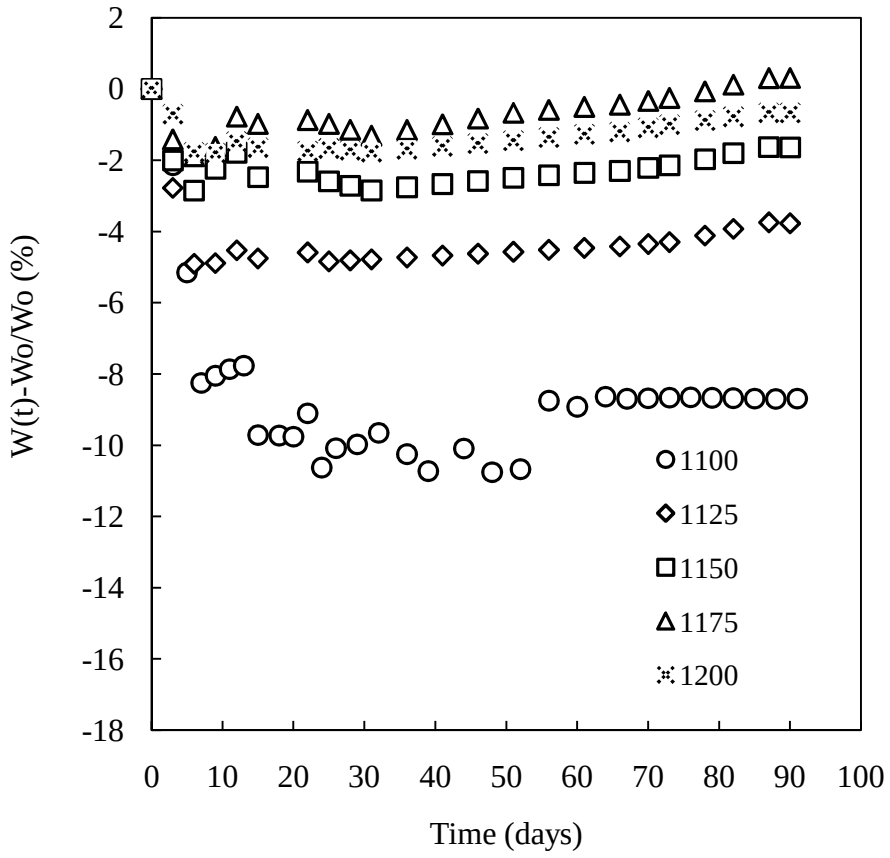

Figure 29 Dissolution behavior of samples made out of the same HA:βTCP=60:40 and sintered at T= 1100°C, 1125°C, 1150°C, 1175°C, and 1200°C

4.3.4 Modeling of CaS Dissolution

The weight evolution of CaS filled samples suggests that the filler phase dissolves rapidly and exposes the underlying HA:βTCP scaffold as it recedes. Such behavior is expected given the relatively high dissolution rate of CaS. In Figure 30, the normalized mass evolution of the three mixtures of HA:βTCP, each filled with CaS, is shown.

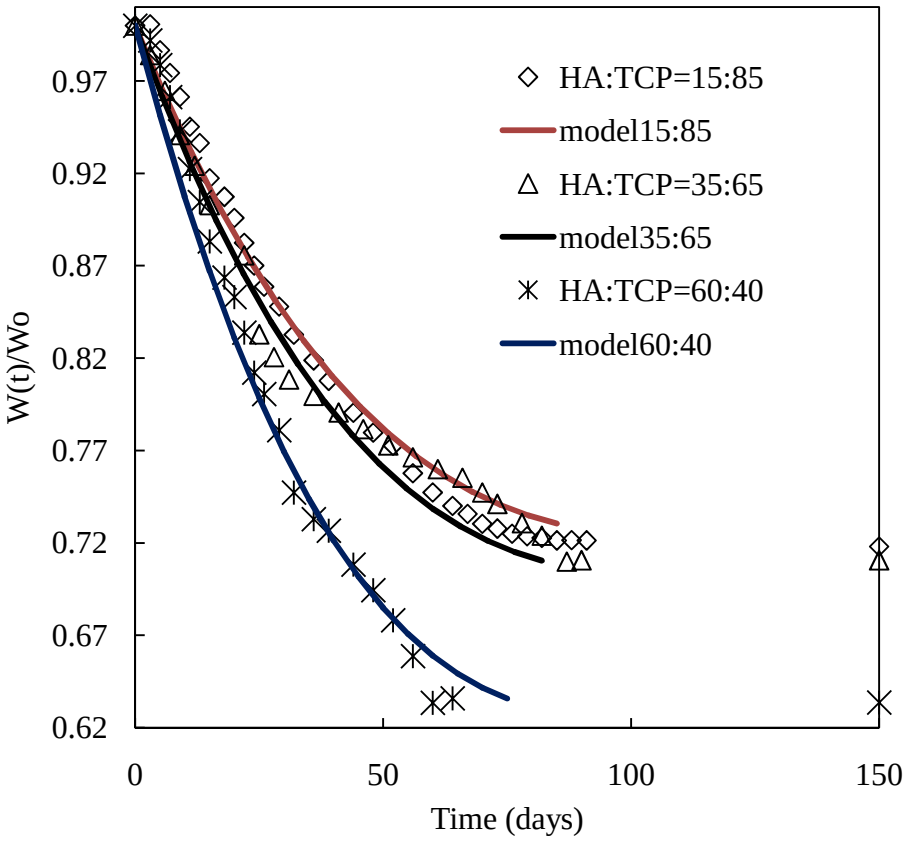

Figure 30 Dissolution of the CaS filled samples

The CaS filling was considered to be the shape of a disk with the initial dimensions of 5.5mm radius and 3mm height. The CaS is assumed to dissolve from one face and the sides of the disk with a constant linear rate of $v=dx/dt$. Note that the sample dimensions imply that $x \leq 3$ mm. The mass of the disk as a function of time ($m_{CaS}(t)$) may be written as:

$$m_{CaS}(t) = \rho\pi(R_o - vt)^2(h_o - vt) \qquad (6)$$

where: $x = x(t) = vt;\ x(0) = 0$; R_o=5.5mm; h_o=3mm.

Note: at t=0, $m_{CaS}(0) = \rho \pi R_o^2 h_o$.

The mass of the CaS filled sample is then the mass of the HA:βTCP scaffold plus the mass of the CaS disk. Here, the rate of dissolution of the scaffold is assumed to be much less than that of the CaS and that the fraction of the scaffold exposed to the simulated body fluid is only that where the CaS disk has receded to reveal the scaffold. Also, since the scaffold interpenetrates with the CaS disk, the volume (mass) of CaS is the total volume (mass) of the sample minus the volume of the ceramic. Given these assumptions, the time dependent mass of the sample is:

$$\left.\begin{aligned} m_s(t) &= m_{CaS}(t) + m_{HA:\beta TCP} \\ t &< \frac{3}{v} \end{aligned}\right\}$$

$$\left.\begin{aligned} m_s(t) &= m_{HA:\beta TCP} \\ t &> \frac{3}{v} \end{aligned}\right\}$$

In Figure 30, the normalized mass $m_s(t)/m_s(0)$ is plotted as a function of time for quadrant samples of various scaffold composition. For the HA:βTCP=15:85 sample, the $m_s(0)$≈0.294g, $m_{HA:\beta TCP}$≈0.798g and $v_{15:85}$≈0.25mm/week. For the HA:βTCP=35:65 sample, the $m_s(0)$≈0.21g, $m_{HA:\beta TCP}$=0.512g and $v_{35:65}$≈0.26mm/week. For the HA:βTCP=60:40 sample, the $m_s(0)$≈0.296g, $m_{HA:\beta TCP}$=0.516g and $v_{60:40}$≈0.28mm/week.

The variation in calculated erosion rate of the CaS for the three sample compositions tested is small, but seems to increase with the amount of HA in the scaffold. One possible explanation is that the βTCP rich scaffolds partially dissolve along with the CaS. Since the SBF is only changed every second day, it is likely that a saturation limit of Ca^{2+} is achieved over a much shorter time period. If this is the case, the actual dissolution time between SBF refreshing is less than the two days and corresponds

to the total rate of Ca^{2+} dissolving. If the scaffold contributes to the Ca^{2+} concentration, this would effectively slow the rate of CaS dissolution as observed in the results.

The other filling tested, Ch, behaved like a barrier between the ceramic and the SBF. A good explanation is that the *in vitro* environment does not possess the right mechanism for Ch to solubilize. At pH 7.2-7.4, Ch is insoluble and there are no enzymes (lysozyme) present in the solution. The Ch filling assay is not conclusive and it is believed that the assay should be repeated providing the right enzyme in the simulated body fluid.

CHAPTER 5

5.0 CONCLUSIONS AND FUTURE WORK

In this thesis, the formulation and printing of colloidal inks of hydroxyapatite and β tri-calcium phosphate ceramics to assemble synthetic bone scaffolds is presented. The ceramic processing from powder to sintered scaffold with designed porosity across multiple length scales is described and characterization data is presented. A novel approach of filling the macroscopic pore structure with highly soluble calcium sulfate filler for preventing blood clotting during early implantation was conceived and tested by *in vitro* dissolution studies. This chapter reflects on the entirety of the project and ties the results and discussion back to the hypotheses postulated in Chapter 2. This chapter also presents some ideas for future work to continue the investigation of the artificial bone scaffolds.

5.1 Conclusions about Hypotheses Statements

5.1.1 Hypothesis 1

Positive affirmation of the first hypothesis is clearly supported by the results. Namely, a three dimensional binary hydroxyapatite and beta tri-calcium phosphate structures can be fabricated using high particle concentration printable aqueous inks and the green body successfully sintered with both minerals present in the final product. A consistent and rapid method of processing as-received ceramic powder results in successfully formulated inks for robocasting. Single-material inks and binary inks are formulated by mixing different proportions of single material inks. It is observed that a mixture of two printable inks can be combined in any proportion to result in a new

printable ink. However, the precise dosage of each ink in the mixture is sensitive and a more controllable approach of simply formulating an ink using both HA and βTCP ceramic powders in appropriate amounts is used as the preferred method. The mineral composition of the HA and βTCP powders before and after calcinations is confirmed via X-ray diffraction. The mineral composition of the samples built from mixtures of the two materials after sintering shows clear existence of both minerals in the 60:40 samples. In the 15:85 samples the HA-specific peaks are muted: masked by those for the βTCP. HA phase is unlikely transformed to βTCP due to the stoichiometry and low processing temperature.

5.1.2 Hypothesis 2

The second hypothesis states that the dissolution behavior of the scaffolds is a function of the proportions of HA and βTCP. The *in vitro* dissolution studies demonstrate that the higher the concentration of βTCP, the greater the mass loss of the scaffold and that dissolution occurs at a slightly faster rate in high βTCP samples. Precipitation of bio-apatite due to a relatively small fluid volume during the dissolution study allows for some weight gain in high surface area samples. This masks the expected higher dissolution rate one would expect with a high surface area. This phenomenon would likely be mitigated were the dissolution study performed in a continuously flowing system of fresh fluid.

5.1.3 Hypothesis 3

The third hypothesis is confirmed by the results in that sintering shrinkage, density, porosity and dissolution behavior are all functions of the sintering time and temperature. The high temperature (1175, 1200^{o}C) treated samples display the greatest linear shrinkage, least porosity and lowest mass loss during dissolution.

5.1.4 Hypothesis 4

Microporosity is controlled by inclusion of a fugitive porogen in the ceramic ink formulation and partially confirms hypothesis four. The increased microporosity is verified by microscopy and density measurements. The statement that increased porosity increases the rate of dissolution is not supported by the data presented in this thesis. The samples studied show less dissolution than similarly sintered samples without the pore forming inclusion. It appears that the increased surface area of the highly porous samples allows for rapid dissolution and repid achievement of saturated conditions in the simulated body fluid followed by precipitation of stable bio-apatite. This conjecture is supported by electron microscopy results that show precipitates of a second phase after only five days in simulated body fluid.

5.1.5 Hypothesis 5

The fifth hypothesis that a CaS filler phase will rapidly dissolve followed by dissolution of the underlying scaffold is confirmed by the data. The CaS filler dissolved entirely in a period of approximately 75 days in all samples studied. The composition of the sample plays a secondary role as since the bulk of the mass loss is due to CaS dissolution. The dissolution rate of CaS is modeled by a surface erosion process where the underlying scaffold minimally influences the rate of dissolution. The linear rate of surface erosion varies between 0.25 to 0.28 mm/week.

5.2 Future Work

The *in vitro* results presented in this thesis are in agreement with the expected trends that were hypothesized from the outset of the project. However, further quantification to reveal specific dissolution rates for the various scaffold configurations

(*i.e.*, composition, state of microporosity, and filler phase) need to be performed. The model of surface erosion of the CaS filler seems plausible, but one may question the effect of the relatively small reservoir volume of simulated body fluid and infrequent changing this fluid on the accuracy of the calculated dissolution rate. This effect is also apparently present in the highly microporous samples where a more rapid dissolution rate is expected. To quantify this effect, a new experiment should be conducted where the volume of SBF is significantly increased such that the activity of Ca^{2+} remains relatively constant throughout the dissolution time. This could be achieved by calculation of the total quantity of Ca available in the CaS filler and the underlying HA:βTCP scaffold. Additionally, the reservoir should be stirred so that the conditions for dissolution could be accurately modeled as a constant solution concentration.

APPENDIX

A1. Two-ink printing

For two ink printing two syringes attached to the z-axis of the robot are used. Two rigid plastic tubes transported the ink from the syringes to the two deposition nozzles. The software permits the alignment of the two nozzles on the x-y plane so they are approximately at the same level horizontally and at a known distance from one another. Structures are built from two materials in layer-by-layer fashion, one layer printed of one material being superposed on one layer fabricated from the other material. After printing, scaffolds are extracted from the oil bath together with the ceramic plate that served as substrate and allowed to drain of oil and dry at 80^{o}C in the low temperature oven (Oakton Stable Temp, Cole-Parmer). When dry, the scaffolds are transferred to a different porous ceramic surface and introduced in the furnace (Model LH3 02/17, Nabertherm, Germany) for heat treatment.

A special case constitutes when binary lattices made out of ceramic and a fugitive ink layers are co-fired. Rice starch ink burns out in the temperature interval from 175^{o}C to 275^{o}C as determined in thermo-gravimetric analysis. The firing program was modified to include a slow 6 hours burnout of the fugitive ink. Steps included first a 5.83^{o}C/min heating to 175^{o}C, then a 0.27^{o}C/min ramp until 275^{o}C, heating at 4.16^{o}C/min to 400^{o}C, isothermal hold at 400^{o}C for 1 h, 8.33^{o}C/min ramp until 900^{o}C, isothermal hold at 900^{o}C for 2 h, 5^{o}C/min heating to 1200^{o}C, another isothermal hold at 1200^{o}C for 4 hours, and then cooling to room temperature at 5^{o}C/min.

The resulted lattices after firing contain only one material, the second one being burned out during heat treatment. Figure 31 shows optical microscope images of this kind

of lattices. The round–shaped gaps in the lateral view (Figure 31b) and section (Figure 31c) are where the fugitive ink's filaments were located before firing.

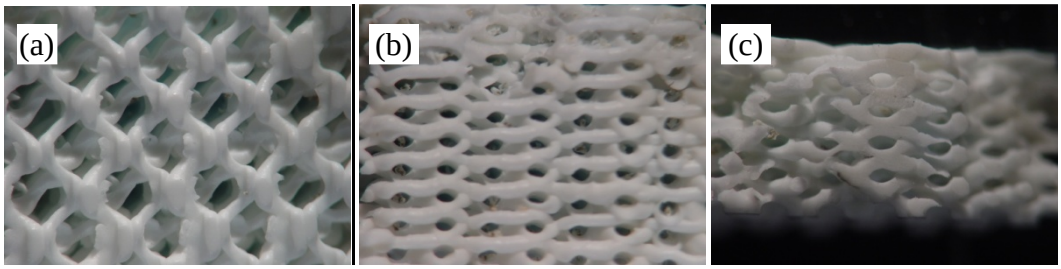

Figure 31 Optical microscope images of a rice starch/ HA:βTCP binary lattice after sintering: a) top view of the ceramic lattice after sintering at 1200oC for 4 hours, b) lateral view of the same structure, c) diagonal section through the ceramic structure (4x magnification)

The matching of two very different inks for printing and after that for heat treatment was faced when building and firing the layered ceramic/rice starch sine-wave samples (Figure 31). The rice starch ink is probably not the best candidate for support material because it shrinks significantly while drying, creating numerous defects into the ceramic. These defects don't totally "heal" during sintering. A very long and slow burn-out of the rice starch partially solved the problem. Still, a fugitive ink that does not shrink significantly during the drying process and burns out at a temperature where ceramics begin already densification would be ideal. A good candidate would be a carbon black ink.

For ceramic-ceramic two-ink printed structures, optical microscopy was used to observe the overall aspect of the different layers, and occurrence of different defects as well. In Figure 32 the light blue layers are made out of HA, while the white ones are made out of βTCP. Defects, like not perfect superposition of layers, can be observed in Figure 32 b) below.

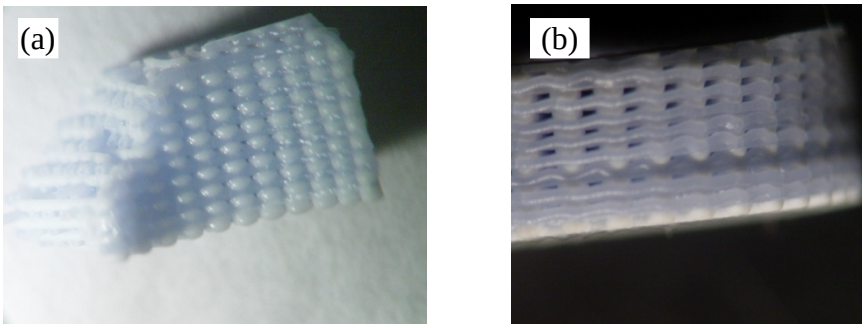

Figure 32 Optical microscope image of HA &βTCP structure made by alternate layer deposition for quality assessment: (a) inside of a round structure, (b) outside view of a round sample

A2. Robocasting gallery

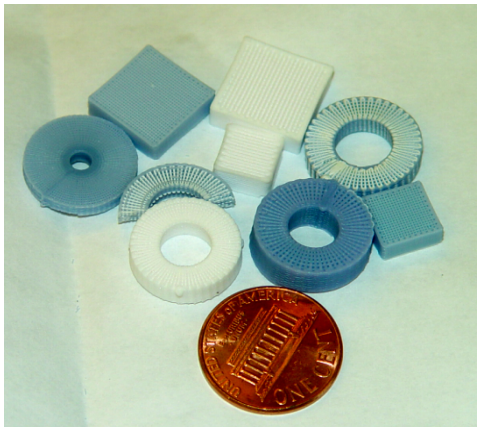

Figure 33 Photograph of various simple geometries of different HA:βTCP mixtures. The darkest shade of blue object is made entirely out of HA, the white objects are made out of βTCP, and the intermediate shades of blue are made out of mixtures of HA and TCP

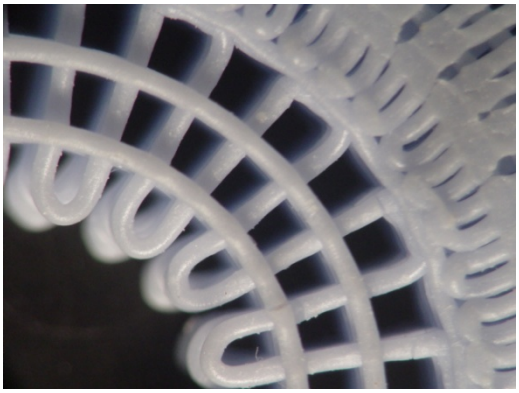

Figure 34 Photograph of round structure with varied meso-porosity

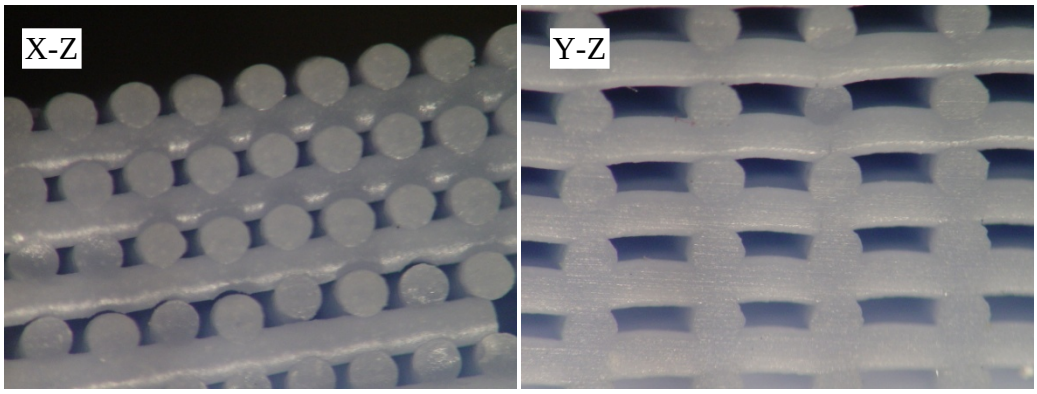

Figure 35 Photograph of two sections through a HA structure: XZ plane left, YZ plane right

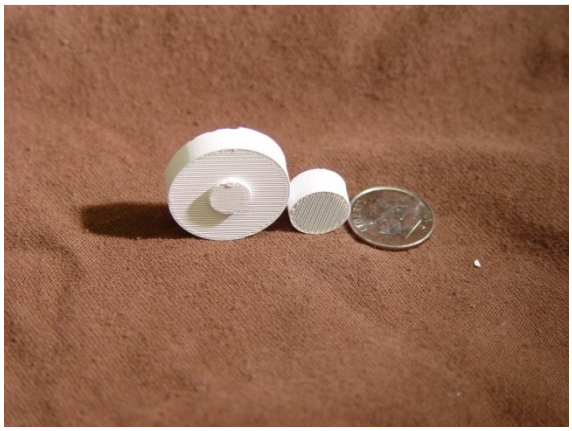

Figure 36 Photograph of samples used in the 3D profusion study

Figure 37 Photograph of samples used in the animal study

REFERENCES

1. Cowin, S.C., *Bone mechanics handbook / edited by Stephen C. Cowin*. 2001, Boca Raton, FL : CRC Press, 2001.
2. Jacobs, C.R., *Bone mechanics handbook (second edition): Stephen C. Cowin (Ed.); CRC Press, Boca Raton, FL, 2001, hardback ISBN 0-8493-9117-2.* Journal of Biomechanics, 2002. **35**(5): p. 723-724.
3. Mamidwar, S.S., et al., *In vitro characterization of a calcium sulfate/PLLA composite for use as a bone graft material*. 2007. p. 57-65.
4. Carson, J.S. and M.P.G. Bostrom, *Synthetic bone scaffolds and fracture repair.* Injury, 2007. **38**(1, Supplement 1): p. S33-S37.
5. Stocum, D.L., *Regenerative biology and engineering: strategies for tissue restoration.* Wound Repair And Regeneration: Official Publication Of The Wound Healing Society [And] The European Tissue Repair Society, 1998. **6**(4): p. 276-290.
6. Okii, N., et al., *In vivo histological changes occurring in hydroxyapatite cranial reconstruction - Case report.* Neurologia Medico-Chirurgica, 2001. **41**(2): p. 100-104.
7. Hirano, S., et al., *Use of hydroxyapatite for reconstruction after surgical removal of intraosseous hemangioma in the zygomatic bone.* Plastic and Reconstructive Surgery, 1997. **100**(1): p. 86-90.
8. Mercier, P., et al., *Long-term stability of atrophic ridges reconstructed with hydroxylapatite: A prospective study.* Journal of Oral and Maxillofacial Surgery, 1996. **54**(8): p. 960-968.
9. H., D., *Versuch über Knochenplombierung bei höhlenförmigen Defekten des Knochens.* Beitr Klin Chir, 1892. **9**: p. 804-810.
10. Orsini, G., et al., *Bone-defect healing with calcium-sulfate particles and cement: an experimental study in rabbit.* Journal Of Biomedical Materials Research. Part B, Applied Biomaterials, 2004. **68**(2): p. 199-208.
11. Raffy Mirzayan, V.P., Raffi Avedian, Deborah M. Forrester and Lawrence R. Menendez, *The Use of Calcium Sulfate in the Treatment of Benign Bone Lesions: A Preliminary Report.* The Journal Of Bone And Joint Surgery. American Volume, 2001. **83A**: p. 355-358.
12. Lee, J.-Y., et al., *Enhanced bone formation by controlled growth factor delivery from chitosan-based biomaterials.* Journal of Controlled Release, 2002. **78**(1-3): p. 187-197.
13. Petite, H., et al., *Tissue-engineered bone regeneration.* Nature Biotechnology, 2000. **18**(9): p. 959-963.
14. Boyan, B.D., et al., *Role of material surfaces in regulating bone and cartilage cell response.* Biomaterials, 1996. **17**(2): p. 137-146.
15. Haddad, R.J., Jr., S.D. Cook, and K.A. Thomas, *Biological fixation of porous-coated implants.* The Journal Of Bone And Joint Surgery. American Volume, 1987. **69**(9): p. 1459-1466.

16. Thomas, K.A., et al., *THE EFFECT OF SURFACE MACROTEXTURE AND HYDROXYLAPATITE COATING ON THE MECHANICAL STRENGTHS AND HISTOLOGIC PROFILES OF TITANIUM IMPLANT MATERIALS.* Journal Of Biomedical Materials Research, 1987. **21**(12): p. 1395-1414.
17. Otsuki, B., et al., *Pore throat size and connectivity determine bone and tissue ingrowth into porous implants: three-dimensional micro-CT based structural analyses of porous bioactive titanium implants.* Biomaterials, 2006. **27**(35): p. 5892-5900.
18. Descamps, M., et al., *Synthesis of macroporous [beta]-tricalcium phosphate with controlled porous architectural.* Ceramics International. **In Press, Corrected Proof**.
19. Christopher J. Damien, J.R.P., *Bone graft and bone graft substitutes: A review of current technology and applications.* Journal of Applied Biomaterials, 1991. **2**(3): p. 187-208.
20. Calvert, J.W., L.E. Weiss, and M.J. Sundine, *New frontiers in bone tissue engineering.* Clinics In Plastic Surgery, 2003. **30**(4): p. 641.
21. Hench, L.L., *Bioceramics: From Concept to Clinic.* Journal of the American Ceramic Society, 1991. **74**(7): p. 1487-1510.
22. Bandyopadhyay, A., et al., *Calcium phosphate-based resorbable ceramics: influence of MgO, ZnO, and SiO/sub 2/ dopants.* Journal of the American Ceramic Society, 2006. **89**(9): p. 2675-2688.
23. Miranda, P., et al., *Sintering and robocasting of [beta]-tricalcium phosphate scaffolds for orthopaedic applications.* Acta Biomaterialia, 2006. **2**(4): p. 457-466.
24. Saiz, E., et al., *Preparation of porous hydroxyapatite scaffolds.* Materials Science and Engineering: C, 2007. **27**(3): p. 546-550.
25. Mayer, I., et al., *TEM study of the morphology of Mn2+-doped calcium hydroxyapatite and [beta]-tricalcium phosphate.* Journal of Inorganic Biochemistry, 2008. **102**(2): p. 311-317.
26. Elliott, J.C., *Structure and chemistry of the apatites and other calcium orthophosphates*. 1994.
27. Liu, C., et al., *Kinetics of hydroxyapatite precipitation at pH 10 to 11.* Biomaterials, 2001. **22**(4): p. 301-306.
28. Bouler Jm, L.R.Z.D.G., *Biphasic calcium phosphates: Influence of three synthesis parameters on the HA/beta-TCP ratio*. 2000. p. 680-684.
29. Legeros, R.Z., *VARIABILITY OF HAP/B-TCP RATIOS IN SINTERED APATITES.* Journal of Dental Research, 1986. **65**: p. 292-292.
30. LeGeros, R.Z., *Biodegradation and bioresorption of calcium phosphate ceramics.* Clinical Materials, 1993. **14**(1): p. 65-88.
31. Bouler, J.M., R.Z. LeGeros, and G. Daculsi, *Biphasic calcium phosphates: influence of three synthesis parameters on the HA/beta-TCP ratio*. 2000. p. 680-4.
32. Daculsi, G., et al., *Transformation of biphasic calcium phosphate ceramics in vivo: ultrastructural and physicochemical characterization.* Journal Of Biomedical Materials Research, 1989. **23**(8): p. 883-894.
33. Julien, M., et al., *Physico-chemical-mechanical and in vitro biological properties*

of calcium phosphate cements with doped amorphous calcium phosphates. Biomaterials, 2007. **28**(6): p. 956-965.
34. Yaszemski, M.J., et al., *Evolution of bone transplantation: molecular, cellular and tissue strategies to engineer human bone.* Biomaterials, 1996. **17**(2): p. 175-185.
35. Seol, Y.J., et al., *Chitosan sponges as tissue engineering scaffolds for bone formation.* Biotechnology letters, 2004. **26**: p. 1037-1041.
36. Qingling, F., et al., *Collagen-based scaffolds reinforced by chitosan fibres for bone tissue engineering.* Polymer International, 2005. **54**(7): p. 1034-1040.
37. Agboh Oc, Q.Y., *Chitin and chitosan fibers*. 1997. p. 355-365.
38. Strocchi, R., et al., *Bone regeneration with calcium sulfate: evidence for increased angiogenesis in rabbits.* The Journal Of Oral Implantology, 2002. **28**(6): p. 273-278.
39. *Plaster-of-Paris Fills Bone Voids*. 1999.
40. Rosenblum, S.F., et al., *Diffusion of fibroblast growth factor from a plaster of Paris carrier.* Journal Of Applied Biomaterials: An Official Journal Of The Society For Biomaterials, 1993. **4**(1): p. 67-72.
41. http://en.wikipedia.org/wiki/Calcium_sulfate. *Calcium sulfate.*
42. Bhat, S., *Biomaterials*. 2002: Kluwer Academic Publishers, Narosa Publishing House. 253.
43. Bhat, S., *Resorbable ceramics*, in *Biomaterials*. 2002, Kluwer Academic Publishers, Narosa Publishing House: New Delhi, India. p. 46-47.
44. Hin, T.S., *Chitin-based Biomaterials*, in *Engineering Materials for Biomedical Applications*. 2004, World Scientific. p. 11.1-16.
45. *14.3.3. Scaffold fabrication techniques*, in *Introduction to Biomaterials*, D. Shi, Editor. 2006, Tsinghua University Press, World Scientific. p. 216-220.
46. Li, W.-J., et al., *Fabrication and characterization of six electrospun poly([alpha]-hydroxy ester)-based fibrous scaffolds for tissue engineering applications.* Acta Biomaterialia, 2006. **2**(4): p. 377-385.
47. Akira Myoui, N.T., Masataka Nishikawa, Hideki Yoshikawa, *Three dimensionally engineered hydroxyapatite ceramics with interconnected pores as a bone substitute and tissue engineering scaffold*, in *Biomaterials in ortopedics*, D.T. Michael Yaszemski, Kai-Uwe Lewandrowski, Editor. 2004, Marcel Dekker, Inc.: New York, Basel. p. 287-300.
48. Chun-Jen Liao, C.-F.C.J.-H.C.S.-F.C.Y.-J.L.K.-Y.C., *Fabrication of porous biodegradable polymer scaffolds using a solvent merging/particulate leaching method.* Journal Of Biomedical Materials Research, 2002. **59**(4): p. 676-681.
49. Nam, Y.S. and T.G. Park, *Biodegradable polymeric microcellular foams by modified thermally induced phase separation method.* Biomaterials, 1999. **20**(19): p. 1783-1790.
50. Leong, K.F., C.M. Cheah, and C.K. Chua, *Solid freeform fabrication of three-dimensional scaffolds for engineering replacement tissues and organs.* Biomaterials, 2003. **24**(13): p. 2363-2378.
51. Bellini, A., L. Shor, and S.I. Guceri, *New developments in fused deposition modeling of ceramics.* Rapid Prototyping Journal, 2005. **11**(4): p. 214-220.

52. Kalita, S.J., et al., *Development of controlled porosity polymer-ceramic composite scaffolds via fused deposition modeling.* Materials Science and Engineering: C, 2003. **23**(5): p. 611-620.
53. Chen, Z., et al., *Fabrication of osteo-structure analogous scaffolds via fused deposition modeling.* Scripta Materialia, 2005. **52**(2): p. 157-161.
54. Russias, J., et al., *Fabrication and in vitro characterization of three-dimensional organic/inorganic scaffolds by robocasting.* Journal Of Biomedical Materials Research. Part A, 2007. **83**(2): p. 434-445.
55. Blom, A., *(V) Which scaffold for which application?* Current Orthopaedics, 2007. **21**(4): p. 280-287.
56. Giannoudis, P.V., H. Dinopoulos, and E. Tsiridis, *Bone substitutes: An update.* Injury, 2005. **36**(3, Supplement 1): p. S20-S27.
57. Hutmacher, D.W., *Scaffolds in tissue engineering bone and cartilage.* Biomaterials, 2000. **21**(24): p. 2529-2543.
58. Yan, Y., et al., *Layered manufacturing of tissue engineering scaffolds via multi-nozzle deposition.* Materials Letters, 2003. **57**(18): p. 2623-2628.
59. Ren-Haw, C. and L. Chih-Lung, *Fabrication of high-aspect-ratio ceramic microstructures by injection molding with the altered lost mold technique.* Journal of Microelectromechanical Systems, 2001. **10**(1): p. 62-68.
60. Griffith, M.L. and J.W. Halloran, *Freeform fabrication of ceramics via stereolithography.* Journal of the American Ceramic Society, 1996. **79**(10): p. 2601-2608.
61. J.E. Smay, G.M.G.R.F.S.J.C.I.I.I.J.A.L., *Directed Colloidal Assembly of 3D Periodic Structures.* Advanced Materials, 2002. **14**(18): p. 1279-1283.
62. Simon, J.L., et al., *In vivo bone response to 3D periodic hydroxyapatite scaffolds assembled by direct ink writing.* Journal Of Biomedical Materials Research. Part A, 2007. **83**(3): p. 747-758.
63. Nadkarni, S.S., *Design, assembly and characterization of three-dimensional photonic band gap structures fabricated with barium titanate: strontium titanate: barium zirconate mixtures*. 2006. p. 191-p.
64. Ungár, T., *Microstructural parameters from X-ray diffraction peak broadening.* Scripta Materialia, 2004. **51**(8): p. 777-781.
65. Yang, H.Y., et al., *Sintering behaviour of calcium phosphate filaments for use as hard tissue scaffolds.* Journal of the European Ceramic Society, 2008. **28**(1): p. 159-167.
66. Pedro Miranda, A.P., Eduardo Saiz, Antoni P. Tomsia, Fernanado Guiberteau, *Mechanical properties of calcium phosphate scaffolds fabricated by robocasting.* Journal of Biomedical Materials Research Part A: p. 218-227.
67. Walsh, W.R., et al., *Response of a calcium sulfate bone graft substitute in a confined cancellous defect.* Clinical Orthopaedics And Related Research, 2003(406): p. 228-236.
68. Jennifer Dellinger, J.C.I., Russell Jamison, *Robotic deposition of model hydroxyapatite scaffolds with multiple architectures and multiscale porosity for bone tissue engineering.* Journal of Biomedical Materials Research Part A: p. 383-394.

69. Sailon AM, A.A., Clark E, **Cretiu-Vasiliu C**, Smay J, Ricci JL and Warren SM, ***Dynamic cell culture in a flow-perfusion bioreactor prevents core necrosis and improves mineralization in thick 3D tissue-engineered constructs***. *Plastic and Reconstructive Surgery*, 2008 June. **121(6S):49**.
70. Allori AC, N.P., Lin CD, Sailon AM, Clark E, **Cretiu-Vasiliu C**, Smay J, Ricci JL and Warren SM. , ***Carrier-filled solid scaffolds with time-released porosity for endogenous bone engineering***. *Tissue Engineering, Part A*, May 2008. **14(5):817**.
71. Allori AC, S.A., Lin CD, Clark E, Ricci JL, **Cretiu-Vasiliu C**, Smay JE, Warren SM, ***Flow perfusion improves mineralization and maintains uniform cellular distribution in thick 3D scaffolds***. *Bone*, 2008 March. **42(S1):S18**.
72. Allori AC, S.A., Clark E, **Cretiu-Vasiliu C**, Smay J, Ricci JL and Warren SM, ***Dynamic cell culture prevents core necrosis and creates meaningful osteoblastic networks in thick 3D tissue-engineered constructs***. *Tissue Engineering, Part A*, May 2008. **14(5):840**.
73. Lin CD, A.A., Sailon AM, Clark E**, Cretiu-Vasiliu C**, Smay J, Ricci JL and Warren S. , ***Design of solid scaffolds with time-released porosity for endogenous bone engineering***. *Plastic and Reconstructive Surgery*, 2008 June. **121(6S):109.**

VITA

Cornelia E. Cretiu Vasiliu

Candidate for the Degree of

Master of Science

Thesis: ASSEMBLY OF HYDROXY APATITE: β TRICALCIUM PHOSPHATE: CALCIUM SULFATE BONE ENGINEERING SCAFFOLDS

Major Field: Chemical Engineering

Biographical

Personal Data: Born in Baia Mare, Maramures, Romania, on November 11, 1974, the daughter of Elisabeta and Corneliu-Ionel Vasiliu. Married with Lucian Cretiu Vasiliu

Education: Graduated from Theoretical High School "Liviu Rebreanu", Bistrita, Bistrita-Nasaud, Romania in June 1993; received a General Nursing degree from Professional Nursing School, Targu Mures, Mures, Romania, in June 1997; received Bachelor of Science and Engineering of Oxidic Materials from "Babes-Bolyai" University, Cluj-Napoca, Cluj, Romania in June 2001.Completed the requirements for the Master of Science in Chemical Engineering at Oklahoma State University, Stillwater, Oklahoma in December, 2008.

Experience: Employed by "Sprint Computers Romania" as Local Area Manager in 2001; employed by "CRISTIRO" S.A. Bistrita as: Process Engineer from 2001-2002, Quality Control Engineer 2002-2003, Export Engineer 2003-2004, and Marketing Engineer 2004-2005; employed by Oklahoma State University, School of Chemical Engineering as Graduate Teaching Assistant and Graduate Research Assistant in 2005 to present.

Professional Memberships: American Association of Dental Research since 2007

Name: Cornelia E. Cretiu Vasiliu Date of Degree: December, 2008

Institution: Oklahoma State University Location: Stillwater, Oklahoma

Title of Study: ASSEMBLY OF HYDROXY APATITE: β TRICALCIUM PHOSPHATE: CALCIUM SULFATE BONE ENGINEERING SCAFFOLDS

Pages in Study: 78 Candidate for the Degree of Master of Science

Major Field: Chemical engineering

Scope and Method of Study: Directed assembly and characterization of composite Hydroxyapatite/βTri-CalciumPhosphate/Calcium Sulfate (HA/βTCP/CaS) scaffolds with designed pore distribution for controlled solubility. Concentrated aqueous colloidal gel ink for extrusion-based direct writing was formulated with commercial HA and βTCP powders blended with, ammonium poly(acrylate) (dispersant), hydroxypropylmethylcellulose (viscosifier), and Polyethyleneimine (flocculant). Prior to ink formulation, HA and βTCP powders were calcined, milled, dried and characterized by X-ray diffraction. Mixtures of HA:βTCP in volumetric ratios of 15:85, 35:65, and 60:40 were formulated as inks. Rice starch was formulated as ink and mixtures ceramic: rice starch blended in volumetric ratios of 85:15, 75:25, and 50:50 were produced. Disk samples (∅11mm × 3mm thick) with an internal lattice structure of 250μm rods spaced by 250 μm or 500 μm in a periodic, open pore network were printed and sintered at 1100, 1125, 1150, 1175, and 1200^{o}C for 4 hours. The control set for each composition and pore structure had empty pores while the two test groups were filled with 2.4% Chitosan gel or Calcium Sulfate (CaS). The scaffolds were immersed in simulated body fluid and weight loss was measured by gravimetric analysis on a three day frequency.

Findings and Conclusions: The assembled three-dimensional, binary HA/βTCP structures can be sintered successfully and have both phases present in the final product. The scaffolds dissolve faster with higher βTCP content and CaS filled scaffolds show dissolution behavior dominated by surface erosion of the filler phase. Micro-porosity induced by porogens does not accelerate the dissolution in vitro. In contrast, chitosan filled samples showed minimal weight loss, attributed to shielding of the βTCP from SBF by the conformal and relatively stable chitosan hydrogel. Designer porous HA-βTCP scaffolds may also include controlled solubility behavior by controlling HA: βTCP ratio and selecting soluble pore filler. CaS may be used as a sacrificial pore filler to retard scaffold dissolution by 75 days, whereas chitosan hydrogel may persist as filler for longer periods.

Professor James E. Smay, Ph.D.